



OPEN

## Upcycling of waste EPS beads to immobilized codoped TiO<sub>2</sub> photocatalysts for ciprofloxacin degradation and *E. coli* disinfection under sunlight

Manasa Manjunatha &amp; Hari Mahalingam

The emerging global problem of antimicrobial resistance needs immediate attention. In this regard, this work demonstrates the use of expanded polystyrene waste in the synthesis of immobilized photocatalytic films for the treatment of antibiotics as well as for bacterial disinfection. A boron–cerium codoped TiO<sub>2</sub> catalyst (of specific composition: B<sub>0.8</sub>Ce<sub>0.2</sub>TiO<sub>2</sub>) was immobilized in an expanded polystyrene (EPS) film prepared from waste EPS beads. These films were studied for the degradation of ciprofloxacin (CIP) and disinfection of *E. coli* under sunlight. The film with a catalyst loading of 20 wt% showed a maximum degradation of 89% in 240 min with a corresponding TOC reduction of 84%. A 7.4 and 6.3 log reduction from the bacterial inactivation studies in the presence and absence of antibiotics, respectively, was obtained. The EPS film was stable after five times of reuse, and no significant chemical changes in the used film were observed from FTIR analysis. The average thickness of the prepared film was found from FESEM analysis to be 1.09 mm. These EPS films were also tested for degradation of other antibiotics, such as norfloxacin, levofloxacin and moxifloxacin. The EPS films were tested in two different reactor volumes at optimum conditions. Also, the effectiveness of B<sub>0.8</sub>Ce<sub>0.2</sub>TiO<sub>2</sub>/EPS film in real water samples indicates its potential in large-scale and real-world applications. Thus, these B<sub>0.8</sub>Ce<sub>0.2</sub>TiO<sub>2</sub>/EPS films can be effectively employed for both degradation of ciprofloxacin and the disinfection of *E. coli* under solar light to solve the increasing problem of antimicrobial resistance.

Only 4% of the total water resources available globally are available as freshwater<sup>1</sup> to meet the needs of an ever-growing population, and even this abundant water resource is under tremendous strain due to industrialization. Thus, it is essential to find effective methods for the reuse of treated wastewater. In this context, the antibiotic residues present in the water bodies are considered as emerging contaminants due to their role in the development of antimicrobial resistance (AMR)<sup>2</sup>. The problem of AMR is increasing rapidly worldwide. Existing conventional wastewater treatment methods cannot completely remove the antibiotic residues<sup>3</sup>, present in very low concentrations ranging from nano to micrograms per litre. Advanced oxidation processes (AOPs) such as photocatalysis can serve this purpose through the generation of powerful hydroxyl radicals to completely degrade the organic pollutant molecules into less harmful products.

To improve the functionality of titanium dioxide (TiO<sub>2</sub>) because of its wider bandgap of 3.2 eV<sup>4,5</sup>, doping is one strategy to achieve a narrowed bandgap and thus permit utilization of visible light for improved photocatalytic activity<sup>6,7</sup>. Researchers have focused on co-doping with two or more elements, each dopant having a unique property promoting or enhancing the photocatalytic activity under visible light<sup>8–11</sup>. Photocatalysts are commonly used in slurry or suspended forms; however, the photocatalyst is difficult to recover post-treatment and reuse, thus limiting its large-scale applications. These limitations can be overcome by immobilising the photocatalyst onto a suitable inert support. The immobilized form of photocatalyst (nanoparticles) can be recovered and reused easily post-treatment with no or minimal loss of nanoparticles<sup>12,13</sup>.

Immobilized/floating forms of photocatalysts increase the feasibility of catalysts in large-scale applications through their facile recovery and thus reduce operational costs<sup>14–16</sup>. Various supports such as cork<sup>17</sup>, perlite<sup>18,19</sup>,

Department of Chemical Engineering, National Institute of Technology Karnataka (NITK) Surathkal, Mangalore, Karnataka 575025, India. ✉email: mhari@nitk.edu.in

polymers<sup>20–29</sup>, glass beads/glass spheres<sup>30–33</sup>, zeolites<sup>34,35</sup>, clay<sup>36,37</sup>, chitosan<sup>38</sup>, and calcium alginate beads<sup>39,40</sup> are available for immobilization of the photocatalysts. The supporting material must provide a large surface area, strongly adhere to the catalyst, must have excellent degradation stability against strong oxidative radicals, and must be able to adsorb pollutants onto its surface for efficient photocatalysis.

Polymers are the most suitable among various supports as they are cost-effective and readily available. Polymers include polyethylene, polystyrene, polyamide, polymethyl methacrylate, polyethylene terephthalate, polyvinyl alcohol, polycaprolactone, polyacrylonitrile, polyvinylidene fluoride<sup>23,41,42</sup>. Polystyrene/expanded polystyrene (EPS) beads are widely used as packaging materials (in food, electronic goods, and other fragile products), thus creating an enormous amount of waste polymers that need to be reused in a circular economy. These waste polymers can be upcycled for the development of floating photocatalysts, thus solving a major environmental problem—‘white pollution’<sup>43–45</sup>. The challenge of lesser accessibility to photons by catalysts in the immobilized form can be overcome through the development of floating photocatalysts which use lightweight material as an inert support for immobilization. This floating property also helps in recycling photocatalysts more easily<sup>12,13,46</sup>. The above-mentioned low-density polymers float on the liquid surface (just below the air–liquid interface), thus ensuring effective utilization of light energy for optimum photocatalytic activity<sup>47</sup>.

In recent years, polystyrene/EPS beads in the form of thin films<sup>48–53</sup> as a support for immobilization have attracted much attention due to their non-toxicity, low cost, and chemical inertness<sup>54</sup>. However, these studies are limited to dyes and disinfection<sup>53,55–57</sup>. Also, these studies have been performed under UV light, as summarized in Table 1 (Supporting Information). Other immobilization studies carried out for the degradation of dyes, antibiotics, and disinfection are summarized in Table 2 (Supporting Information).

So far, very less or no work has been carried out on the degradation of antibiotics and disinfection using boron and cerium codoped photocatalysts and waste polymer support under sunlight. Waste EPS modified into a photocatalytic film was used in the development of a novel reactor for dye wastewater treatment<sup>58</sup>. Also, Varnagaris<sup>59</sup> explored a modification of waste EPS to an adsorbent material for the removal of norfloxacin antibiotic, while in another study, Liu<sup>57</sup> demonstrated the use of non-expanded polystyrene beads for bacterial inactivation. Styrofoam-TiO<sub>2</sub> composite (W-TiEPS)<sup>55</sup> was studied for methylene blue dye removal and Cr (VI) reduction. This work explores the degradation of ciprofloxacin and microbial disinfection of *E. coli* using an immobilized codoped B<sub>0.8</sub>Ce<sub>0.2</sub>TiO<sub>2</sub> photocatalyst. The codoped catalyst was synthesized using the facile EDTA-citrate sol–gel method. Here, 0.8 and 0.2 correspond to the atomic percentage of B and Ce dopants, respectively, and this particular catalyst composition was earlier identified as the best-performing photocatalyst in our laboratory<sup>60</sup>. B is a well-known disinfectant and Ce promotes higher adsorption ability<sup>60</sup>. Therefore this synergy of dopants can serve the purpose of efficient degradation and disinfection under sunlight. The immobilized film is made from waste EPS beads which are lightweight and buoyant. Thus, using this film to carry out the degradation of ciprofloxacin (CIP) antibiotic, *E. coli* disinfection studies both in the absence and presence of CIP and its real water applications will help in the development of a sustainable immobilized photocatalyst for large-scale and real-world applications.

## Materials and methods

**Reagents.** Degussa P25 Titanium dioxide (99.9% pure) is supplied by Evonik (Japan); boric acid (99.5% extra pure), citric acid (99% extra pure), ammonia solution (99% extra pure), EDTA (99% extra pure) were procured from Loba chemicals (Loba Cheme Pvt Ltd., India); cerium nitrate hexahydrate (99% trace metal basis), acetone (99.5% pure) and ciprofloxacin (≥98% HPLC grade) were obtained from Sigma Aldrich Co., USA; L.B. (Luria Bertani) agar and broth were purchased from HiMedia Laboratories Pvt. Ltd., India. Ethanol was procured from Biological Scientific solutions, India. Waste EPS beads were collected from discarded bean bag fillings.

**Preparation of B<sub>0.8</sub>Ce<sub>0.2</sub>TiO<sub>2</sub>/EPS film.** The codoped B<sub>0.8</sub>Ce<sub>0.2</sub>TiO<sub>2</sub> photocatalyst was synthesized using the facile green EDTA-citrate sol–gel method (see Supporting Information Sect. S2, Scheme 1). The photocatalyst solution (catalyst—a certain weight % with respect to the mass of EPS beads used + 8 mL acetone + 2 mL ethanol) was homogenized through sonication for 15 min in an ultrasonic water bath. The solution was then poured into a Petri plate, followed by the addition of 3 g of EPS (expanded polystyrene) beads. The film was left overnight at room temperature for solvent evaporation (Fig. 1). The prepared film was then gently washed with distilled water to remove loosely bound catalyst particles. The specific amounts of solvents used in the preparation are the optimized amounts based on a preliminary evaluation of the degradation performance for the resulting film (see “Effect of solvent and EPS bead quantities” section).

**Characterization.** The B<sub>0.8</sub>Ce<sub>0.2</sub>TiO<sub>2</sub>/EPS film morphology was analyzed using FE-SEM (ZEISS GeminiSEM 300, Oberkochen, Germany) with different magnifications of X100, X500, and X3000. A profilometer measured surface roughness (Taylor Hobson Taly Surf 50, Illinois, U.S.). The XRD analysis (Panalytical Empyrean series 3, Malvern, U.K.) was carried out using Cu Kα (λ = 0.15418 nm) and 2θ range of 5°–80° (with an increment of 0.05°). The composition and chemical states of doped elements were analyzed from XPS (Omicron ESCA+, Chanhassen, U.S.) with an XAl Kα monochromator X-ray source. FTIR-ATR mode (FT-IR Bruker Alpha spectrometer, Bangalore, India) analysis was carried out to determine the functional groups and chemical bonds in the 4000–500 cm<sup>−1</sup> range. A contact angle analyzer (KRÜSS, Drop shape analyzer-DSA 100E, Hamburg, Germany) was used to determine the polarity of the film. The elements leached from the immobilized film were determined using ICP-OES (Agilent Technologies, 5100, California, U.S.). TOC reduction was measured using a TOC analyzer (TOC-V-CSN, Shimadzu, Osaka, Japan). The degraded sample absorbance measurements were recorded using a UV–Vis spectrophotometer (Shimadzu UV-2600, Kyoto, Japan). The degradation products

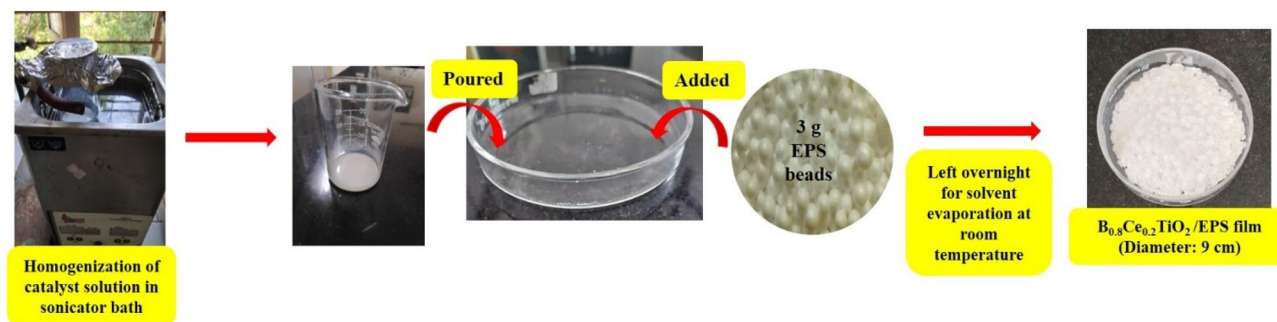


**Figure 1.** Preparation of B<sub>0.8</sub>Ce<sub>0.2</sub>TiO<sub>2</sub>/EPS film using waste EPS beads and catalyst solution (x wt% w.r.t. weight of EPS beads + 8 mL Acetone + 2 mL Ethanol).

were identified using liquid chromatography–mass spectrometry (Shimadzu LCMS-2020, Kyoto, Japan). 10 µL of the degraded sample was injected and then passed through a 5 µm C-18 column (4.6 × 250 mm, column temperature: 30 °C). At a flow rate of 0.5 mL/min, mobile phase A as 0.1% formic acid in acetonitrile and mobile phase B as 0.1% formic acid in water (16:84) was used. The degraded sample was analyzed for 20 min at a wavelength of 280 nm. The characterization of the catalyst employed in this study (Particle size, DLS, DRS etc.) is given in the earlier study<sup>60</sup> and the key results from this work are summarized in Supplementary Information S3 Table 3.

**Photocatalytic studies using B<sub>0.8</sub>Ce<sub>0.2</sub>TiO<sub>2</sub>/EPS film.** *Ciprofloxacin (CIP) degradation.* Before irradiation, the prepared film was immersed into a 200 mL, 10 ppm ciprofloxacin solution and kept under the dark condition to attain adsorption–desorption equilibrium (30 min with constant stirring). The studies were performed generally for 180 min and in some cases for 240 min (12 to 4 p.m.) under sunlight (at NITK Surathkal, latitude: 13° 0′ 40″ N and longitude: 74° 47′ 44″ E). An average light intensity of 80,000 ± 6000 lx and an average temperature of 32 °C were recorded. Samples were collected at intervals of 15 min, and the absorbance values were analyzed using a UV–Visible spectrophotometer at λ<sub>max</sub> of 280 nm. The analysis was performed in duplicates and the error bars represent the standard deviation of measurements.

The CIP degradation and mineralization (% degradation and % TOC reduction) was calculated using Eq. (1). Equation (2) gives the pseudo-first-order reaction constant ( $k$ ) as mentioned in the literature.

$$\% \text{ degradation and } \% \text{ TOC reduction} = \frac{C_0 - C}{C_0} \times 100, \quad (1)$$

$$-\ln \left[ \frac{C}{C_0} \right] = kt, \quad (2)$$

where  $C_0$  &  $C$ —initial and final CIP concentration/TOC,  $t$ —reaction time,  $k$ —rate constant of the reaction.

*Reusability of B<sub>0.8</sub>Ce<sub>0.2</sub>TiO<sub>2</sub>/EPS film.* The stability of the B<sub>0.8</sub>Ce<sub>0.2</sub>TiO<sub>2</sub>/EPS film was determined by reusing the film for five consecutive runs. After each run, the B<sub>0.8</sub>Ce<sub>0.2</sub>TiO<sub>2</sub>/EPS film was gently washed with deionized water and dried overnight at room temperature. For each run (cycle), a freshly prepared CIP solution of 10 ppm was used.

*Determination of point of zero charge (pzc).* The initial and final pH values were noted for each experiment<sup>61</sup> which was carried out for different pH values of 3, 5, 7, 9, and 11. The intersection of two plots (initial and final pH) represents the point of zero charge (pzc). The results are plotted in Fig. 11a and it is seen that the B<sub>0.8</sub>Ce<sub>0.2</sub>TiO<sub>2</sub>/EPS film has the point of zero charge at pH 7.64.

*E. coli disinfection (in absence and presence of antibiotic).* Before use, sterilization of glassware was carried out by autoclaving for 20 min at 15 psi. *E. coli* MTCC 9541 strain (isolated from river Ganga) was selected as the model organism for the study and grown using Luria Bertani broth (60 rpm, 24 h). *E. coli* suspension was obtained by centrifuging at 8000 rpm for 10 min (8 °C). Colonies were counted using standard serial dilution and plate count method. A cell density of 75 × 10<sup>8</sup> CFU (colony forming unit)/mL with a limit of detection of 15 CFU/mL was obtained. The disinfection studies using B<sub>0.8</sub>Ce<sub>0.2</sub>TiO<sub>2</sub>/EPS film were performed in both the absence and presence of antibiotic. The antibiotic resistance assay (see “[Determination of point of zero charge \(pzc\)](#)” section below) was carried out in order to determine the concentration of antibiotic to be used for the disinfection study in the presence of CIP. The batch experiments (200 mL) were carried out for 180 min under sunlight with an initial *E. coli* concentration of 10<sup>8</sup> CFU/mL. And for experiments in the presence of antibiotic, 1 ppm CIP was used as this concentration did not show any bacterial resistance for *E. coli*. Before irradiation, a dark condition was maintained for 30 min. For every 15 min, samples were collected, serially diluted (as required), plated, and kept for 24 h incubation (37 °C) for colony count. The error bars were obtained for the duplicate measurements.

Antibiotic resistance assay. Initially, *E. coli* was tested for its resistance against various concentrations of ciprofloxacin (CIP), namely 1, 5, 10, and 100 ppm, using the spread plate method (Fig. 2). Sterile distilled water was used as the control. Inhibition zones were observed for all concentrations except 1 ppm; thus, resistance was shown by *E. coli* for 1 ppm concentration of CIP. Thus, for the disinfection experiments in the presence of CIP, 1 ppm concentration was used.

## Results and discussion

**Characterization of  $B_{0.8}Ce_{0.2}TiO_2$ /EPS film.** Figure 3a shows the morphology of plain EPS film, unused EPS film with  $B_{0.8}Ce_{0.2}TiO_2$  catalyst particles distributed on the surface of the film. Pores created on the surface of the EPS film are clearly visible, and these pores act as active sites for photocatalytic activity. After reusing the EPS film five times, no significant morphological changes were observed. From the FESEM analysis, an average thickness of 1087  $\mu m$  (Fig. 3b) and an average roughness of 15.4323  $\mu m$  was observed from profilometer measurements.

The XRD spectra of plain EPS film,  $B_{0.8}Ce_{0.2}TiO_2$ /EPS film, before and after five times of reuse are given in Fig. 4. In the plain film, two peaks were observed at  $9.975^\circ$ —amorphous polymer and  $19.625^\circ$ —crystalline polymer<sup>62</sup>. After the catalyst immobilization, crystalline peaks of  $TiO_2$  (anatase and rutile) and cerium peaks were observed ( $TiO_2$ —ICSD no. 9852 (Anatase), 9161 (Rutile) and  $CeO_2$ —ICSD no. 072155). The peaks at  $25.32^\circ$  (101),  $37.01^\circ$  (103),  $37.87^\circ$  (004),  $38.60^\circ$  (112),  $48.09^\circ$  (200),  $54.32^\circ$  (105),  $55.12^\circ$  (211),  $62.73^\circ$  (204),  $68.97^\circ$  (116),  $70.30^\circ$  (220), and  $75.11^\circ$  (215) correspond to anatase  $TiO_2$ <sup>63–65</sup>. The peaks at  $27.46^\circ$  (110),  $36.11^\circ$  (101),  $41.31^\circ$  (111),  $56.72^\circ$  (220), and  $64.04^\circ$  (310) correspond to rutile  $TiO_2$ <sup>65,66</sup>. Cerium peaks were found at  $47.05^\circ$  (220),  $56.72^\circ$  (311), and  $60.22^\circ$  (222)<sup>67–69</sup>. No changes in the XRD pattern were observed after five times of reuse of the film. This indicates that the degree of crystallinity remains unchanged even after exposing the film to sunlight.

Figure 5 shows the FTIR spectra of the plain EPS film, unused film, and film after five times of reuse. The peak at  $3361.75\text{ cm}^{-1}$  corresponds to the O–H stretch. The next peak observed at  $3027.47\text{ cm}^{-1}$  corresponds to the C–H bond of the benzene ring in polystyrene. The third peak at  $2919.71\text{ cm}^{-1}$  is due to C–H stretching vibration. Peaks between  $1597$  and  $1446\text{ cm}^{-1}$  correspond to aromatic C=C bond stretch. The next two peaks at  $751.40\text{ cm}^{-1}$  and  $689.59\text{ cm}^{-1}$  correspond to the aromatic C–H bend. No major chemical changes were observed after five times of reuse of the film. No additional peaks were observed, which suggests the absence of contaminants. Similar results were observed in the literature<sup>70,71</sup>.

From contact angle measurements,  $82.93^\circ$  was measured for the  $B_{0.8}Ce_{0.2}TiO_2$ /EPS film, which indicates that it is hydrophilic.  $TiO_2$  is hydrophilic;  $B_{0.8}Ce_{0.2}TiO_2$  photocatalyst and EPS beads are hydrophobic. After catalyst immobilization, it is seen that the EPS film behaves as hydrophilic.

The composition and chemical states of the  $B_{0.8}Ce_{0.2}TiO_2$  immobilized photocatalyst were determined from XPS analysis. Figure 6a depicts the survey spectra of  $B_{0.8}Ce_{0.2}TiO_2$  immobilized film. The Ti 2p peaks were observed at 458.57 eV (corresponds to  $2p_{3/2}$  orbit) and 464.53 eV (corresponds to  $2p_{1/2}$  orbit) (Fig. 6b) which corresponds to  $Ti^{4+}$ <sup>10</sup>. One O 1s peak was observed at 530.47 eV (Fig. 6c), which corresponds to the surface OH<sup>−</sup> group/lattice oxygen<sup>8,64,72</sup>. A peak at 191.13 eV (Fig. 6d) for B 1s indicates the interstitial lattice position of B, which promotes the reduction of  $Ti^{4+}$  to  $Ti^{3+}$  and  $Ti^{3+}$  facilitates effective separation of photogenerated charges and thus enhances the photocatalytic activity<sup>8,10,73,74</sup>. Two Ce 3d peaks (Fig. 6e) appeared at 884.94 eV and 906.18 eV. This indicates the presence of  $Ce^{4+}$ <sup>10,75</sup>. From the XPS study, the amount of photocatalyst present in the EPS film was quantitatively analyzed (Table 4 of SI), and the actual amount of  $B_{0.8}Ce_{0.2}TiO_2$  photocatalyst present was 19.96 wt%, which is in agreement with the intended catalyst loading (20 wt%).

Leaching of the photocatalyst from the EPS film was studied by subjecting the film to continuous stirring in 200 mL distilled water for 24 h. ICP-OES analysis was used to quantify the concentration of elements leached from the photocatalyst. The results showed minute traces of boron (0.3 ppm) and cerium (0.09 ppm). The Boron concentration values are within the permissible limits specified in the drinking water standards set by WHO (2008)<sup>76,77</sup>. No traces of elemental Ti were observed.

**Optimization of CIP degradation parameters.** *Effect of solvent and EPS bead quantities.* The solvents i.e., acetone and ethanol, were combined in different ratios (10 mL acetone and 8 mL acetone + 2 mL ethanol), and the amount of EPS beads was varied (3 g and 4 g) to check the resulting performance of the EPS film with respect to the degradation of CIP. The degradation efficiency was found to be only 26% for 5 wt% (A1 in Fig. 7)

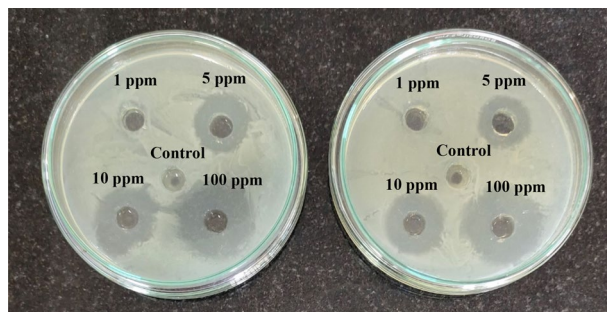
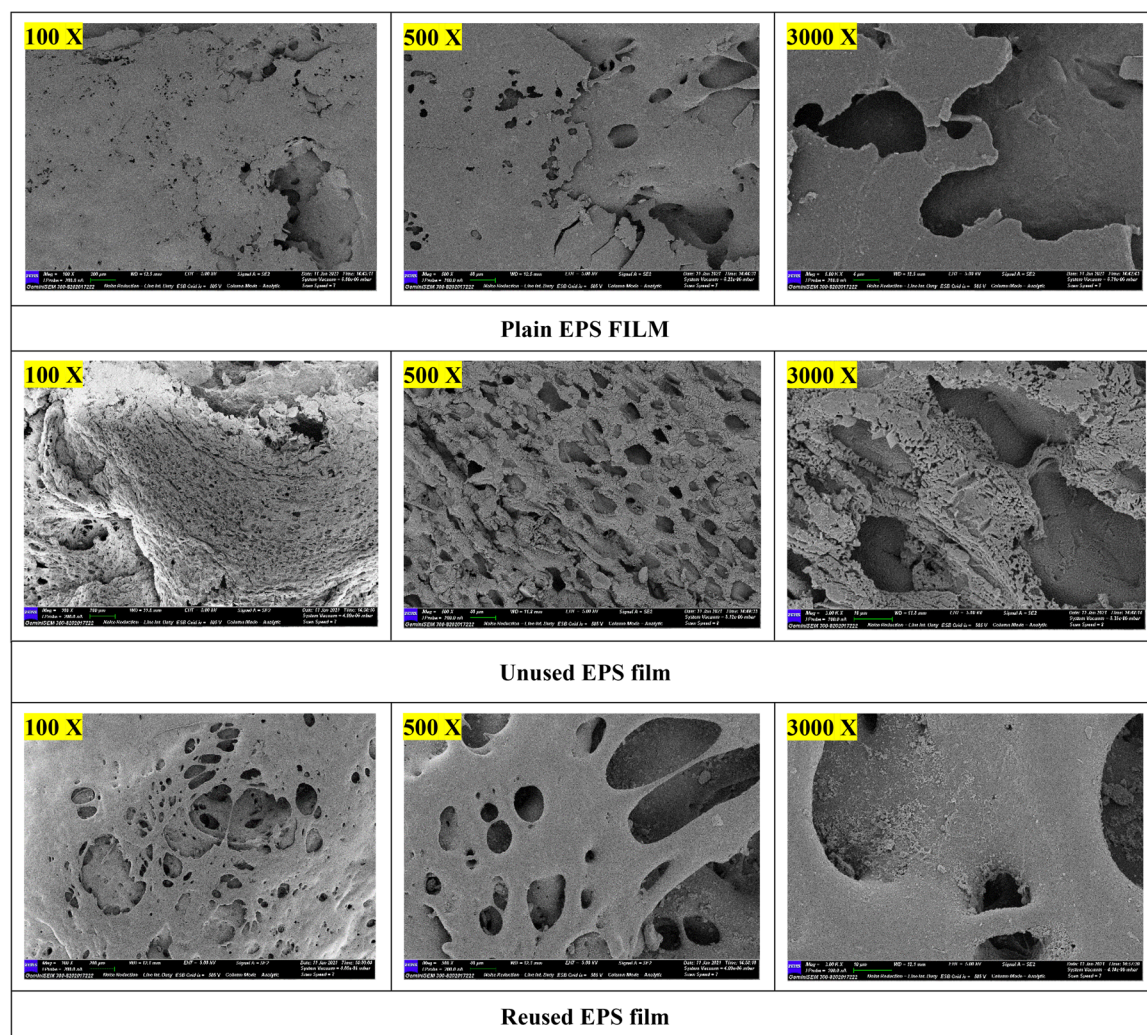
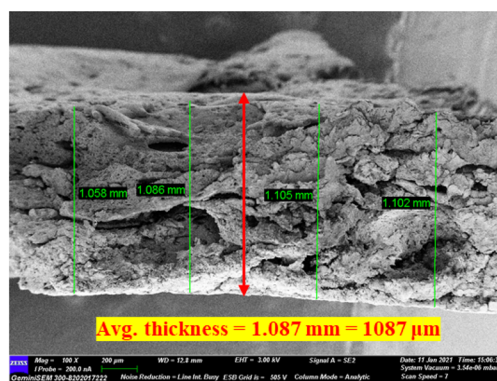


**Figure 2.** Antibiotic resistance assay using *E. coli* and various concentrations of CIP.



(a)



(b)

**Figure 3.** (a) FESEM images of EPS film and film with the immobilized catalyst. (b) Thickness of the  $B_{0.8}Ce_{0.2}TiO_2/EPS$  film.

and 43% for 10 wt% (A2 in Fig. 7) of  $B_{0.8}Ce_{0.2}TiO_2/EPS$  film prepared with 10 mL acetone and 3 g EPS. With the addition of 8 mL acetone and 2 mL ethanol, the degradation efficiency was found to be increasing, with 42% degradation observed for 5 wt% (C1 in Fig. 7) and 57% for 10 wt% (C2 in Fig. 7). Only 27% degradation was observed for the film with 4 g EPS and 10 mL acetone (B1 in Fig. 7). As mentioned in the literature<sup>78</sup>, the degradation increases with an increase in the polarity of the solvent, which is observed in this study after the addition of ethanol. Also, acetone is considered to be less toxic than the other industrial solvents<sup>79</sup>. The presence of pores

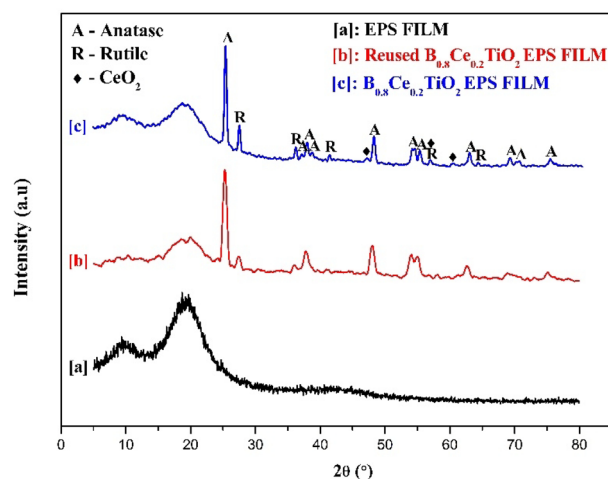


**Figure 4.** XRD spectra of (a) EPS film, (b)  $B_{0.8}Ce_{0.2}TiO_2$ /EPS film after using five times, (c)  $B_{0.8}Ce_{0.2}TiO_2$ /EPS film.

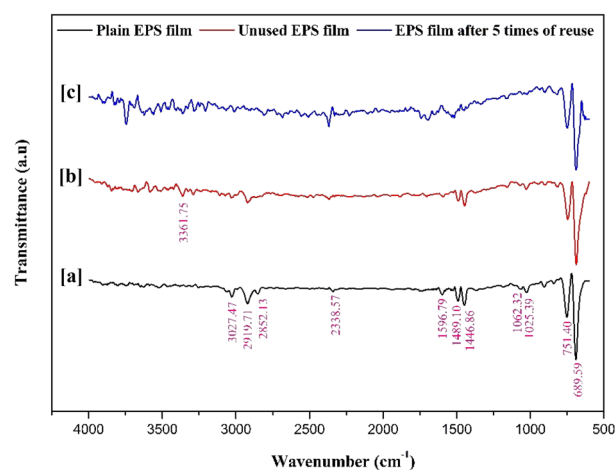


**Figure 5.** FTIR spectra of (a) plain EPS film, (b) unused EPS film, and (c) EPS film after five times of reuse.

(as observed from Fig. 8) indicates the existence of active sites, which helps in achieving higher photocatalytic activity.

**Effect of catalyst dosage.** Photolysis experiments showed only 8.44% degradation of CIP under sunlight, thus indicating the need for further treatment using the  $B_{0.8}Ce_{0.2}TiO_2$ /EPS film. The effect of catalyst dosage on photocatalytic degradation of CIP was examined by varying the catalyst dosage as 5, 10, 15, 20, and 25 wt% (Fig. 9a). A maximum degradation of 81.36% was observed for 20 wt% after 180 min under sunlight. The degradation efficiency of CIP was found to be increasing with an increase in the catalyst dosage up to 20 wt% (optimum catalyst dosage). An increase in the catalyst dosage results in an increase of electron–hole pairs, which in turn improves photocatalytic degradation. However, beyond the optimum catalyst dosage, the degradation decreased due to the reduction in pore size and the number of pores due to the agglomeration of the higher number/excess catalyst particles on the film's surface. Similarly, in the literature<sup>71</sup>, photocatalytic activity has decreased with an increase in the catalyst dosage. Further, for the 20 wt% photocatalytic film, a final degradation of 89.17% (Fig. 9b) was observed at the end of 240 min.

**Effect of CIP initial concentration and kinetic studies.** The effect of CIP initial concentration on the degradation was studied with the optimum catalyst dosage of 20 wt% by varying the initial concentration of CIP in the range of 10 to 40 mg/L, as shown in Fig. 10a. The degradation was found to be decreasing with an increase in antibiotic concentration. With an increase in the CIP concentration, the reactive species (OH radicals) remain constant for a given catalyst dosage and time of irradiation. A higher pollutant concentration requires a higher number of radicals for degradation. Also, more pollutant molecules compete for the same active sites in catalysts, thus

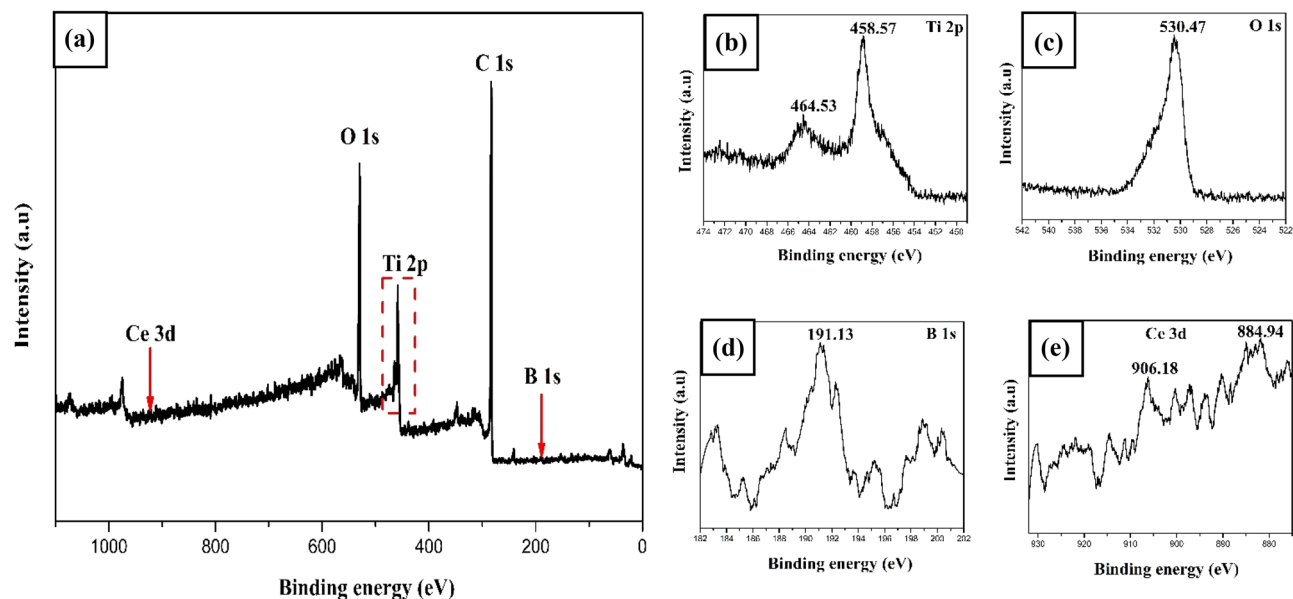


**Figure 6.** (a) XPS analysis of the immobilized  $B_{0.8}Ce_{0.2}TiO_2$  photocatalyst film. (b) Ti spectra, (c) O spectra, (d) B spectra, (e) Ce spectra.

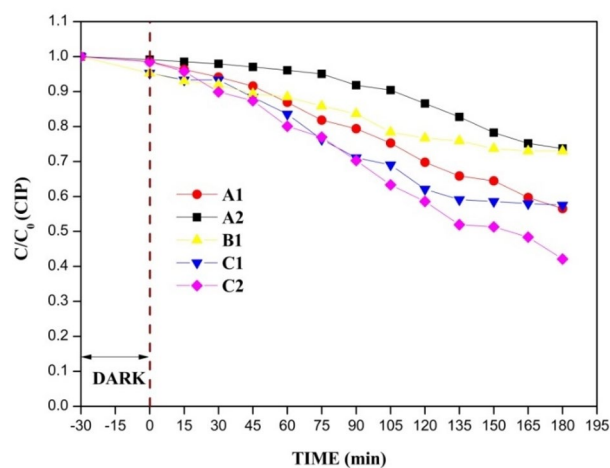


**Figure 7.** Effect of solvents on the photocatalytic degradation of CIP using  $B_{0.8}Ce_{0.2}TiO_2/EPS$  film (A1: 3 g EPS + 10 mL Acetone (5 wt%), A2: 3 g EPS + 10 mL Acetone (10 wt%), B1: 4 g EPS + 10 mL Acetone (5 wt%), C1: 3 g EPS + 8 mL Acetone + 2 mL Ethanol (5 wt%), C2: 3 g EPS + 8 mL Acetone + 2 mL Ethanol (10 wt%).)

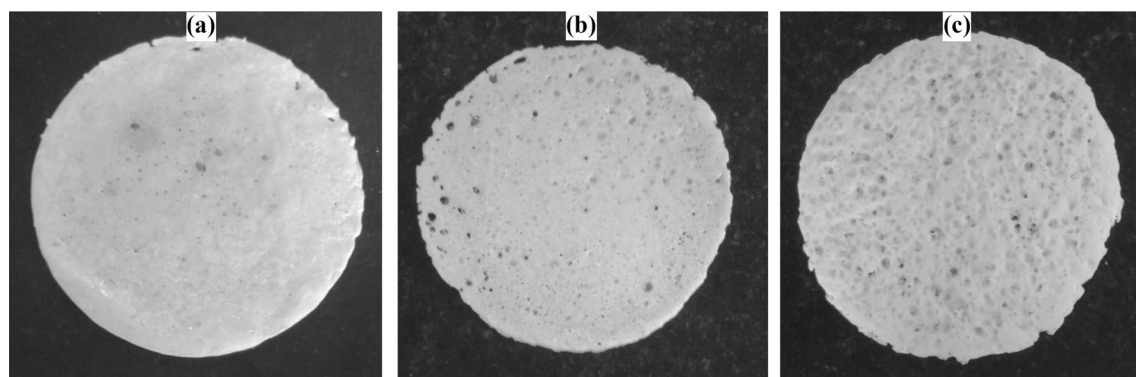


**Figure 8.** EPS films prepared by varying the quantity of EPS and solvents: (a) 3 g EPS + 10 mL Acetone, (b) 4 g EPS + 10 mL Acetone, and (c) 3 g EPS + 8 mL Acetone + 2 mL ethanol.

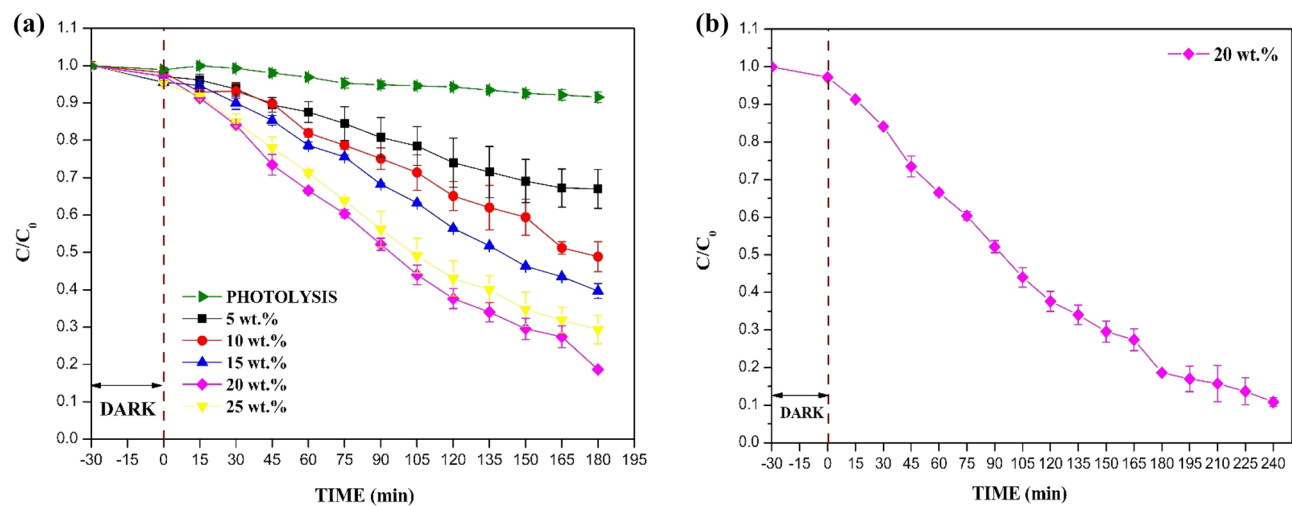


**Figure 9.** (a) Effect of catalyst dosage in immobilized EPS film. (b) Photocatalytic degradation of CIP for 20 wt% EPS film for longer time period. Experimental condition: Initial concentration of CIP = 10 ppm, under sunlight.

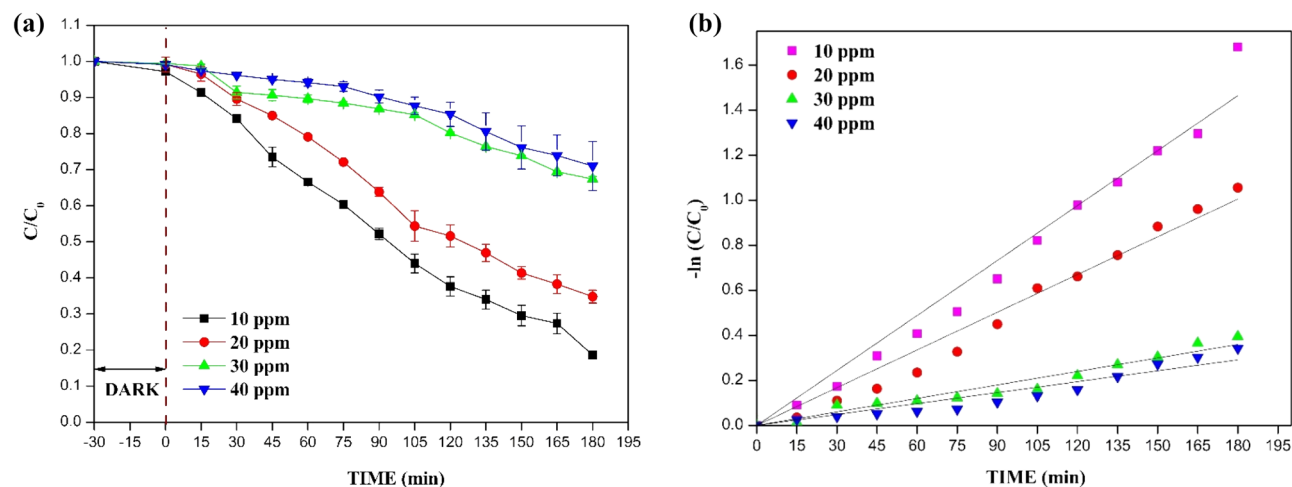


**Figure 10.** (a) Effect of CIP initial concentrations for 20 wt% EPS film, (b) Kinetics plot.

decreasing degradation efficiency. Similarly, in the literature<sup>71</sup>, there is a decrease in the degradation with an increase in the initial concentration of CIP.

The reaction kinetics of CIP degradation for the above different initial concentrations is shown in Fig. 10b. The kinetics of the reaction was found to be pseudo-first-order. The  $k$  and  $R^2$  values are given in Table 5 (Supporting Information—Sect. S4). The rate constant  $k$  values were found to be decreasing with an increase in the initial concentrations of CIP.

**Effect of pH.** The pH of a solution is an important aspect as it determines the properties of the surface charge of the photocatalyst and the adsorption behaviour of pollutant molecules<sup>80,81</sup>. It can affect changes in the ionic state of pollutants, the surface charge of the photocatalyst, and concentrations of reactive oxygen species. Thus, pH greatly influences photocatalytic degradation of the CIP<sup>82–84</sup>. The effect of pH on CIP degradation was studied by varying the pH as 3, 5, 7, 9, and 11 using the optimum conditions of 20 wt% catalyst-loaded film and 10 ppm of CIP for 180 min. pH was adjusted using 1 M HCl and 1 M NaOH. The CIP has two dissociation constant values of  $pK_{a1} = 6.09$  (carboxylic acid group) and  $pK_{a2} = 8.74$  (nitrogen on piperazinyl ring). The point of zero charge of  $B_{0.8}Ce_{0.2}TiO_2$  was found to be 7.64 (Fig. 11a). The CIP degradation was good at both pH 7 and pH 5. From Fig. 11b (the inset figure shows the degradation for different pH values over a period of 180 min), at high pH values (basic pH), both the EPS film and CIP are negatively charged, due to which repulsion occurs, and thus, a lesser degradation happens. The EPS film and CIP are positively charged at low pH values (acidic pH). However, degradation is higher than that at the high pH, which might be due to the higher oxidation potential of hydroxyl radicals for the degradation of organic pollutants at low pH<sup>84</sup>. The pH of rivers and lakes in India lies in the range of 6.5–8.5. Also, the effluent with antibiotic residues from the pharmaceutical manufacturing

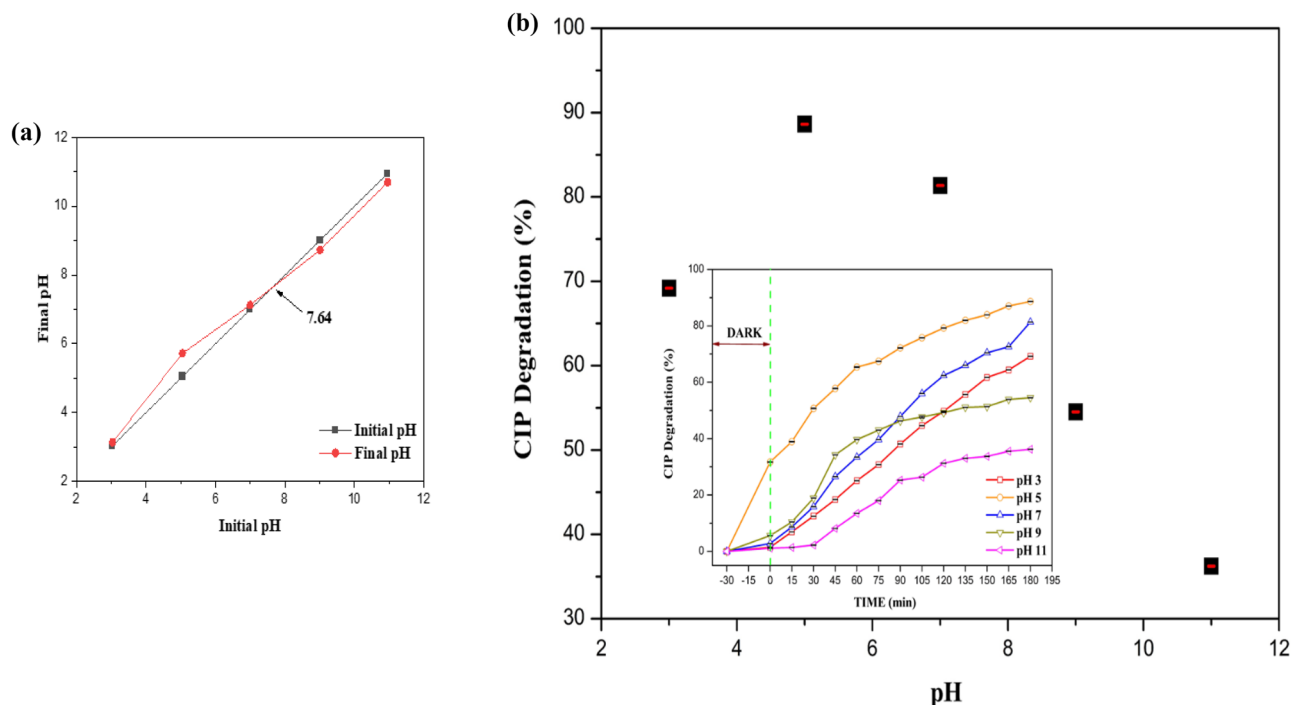


**Figure 11.** (a) Point of zero charge (pzc) of  $B_{0.8}Ce_{0.2}TiO_2/EPS$  film and (b) effect of pH on CIP degradation.

industries or hospital effluent has a pH in the range of 6.7–7.7 (effluent discharge standards for industries and hospitals)<sup>80</sup>. In view of practical and real water sample applications, all the studies were performed at a pH of 7.

**Reusability studies.** Reusability studies of the  $B_{0.8}Ce_{0.2}TiO_2/EPS$  film were performed five times with a degradation time of 180 min for each cycle. After each cycle, the EPS film was washed with distilled water and dried at room temperature (overnight). The degradation efficiency of CIP slightly decreased from 81.36 to 71.15% (Fig. 2, Supporting Information Sect. S5) after five consecutive cycles of reuse, and this decrease is lesser when compared to the suspended form with a ~20% decrease in the degradation efficiency after five times of reuse of the nanoparticles in the earlier study<sup>60</sup>. The slight decrease in degradation efficiency can be attributed to the adsorbed CIP on the surface of the film, which blocks the active sites available for photocatalytic activity. Thus, these results suggest the stability of the  $B_{0.8}Ce_{0.2}TiO_2/EPS$  film and its application for large-scale purposes.

**Analysis of degraded CIP samples.** *TOC analysis and antimicrobial activity of the degraded CIP sample.* The degraded CIP sample showed a TOC reduction of 46.41% after 180 min and 84.41% after 240 min. These results indicate the mineralization of CIP with an increase in the treatment time. Further, the loss of antimicrobial activity of the degraded CIP sample was determined using *E. coli* as the test organism by the agar well diffusion method. The experimental procedure is given in the Supporting Information Sect. S8. As seen from Fig. 3 (Supporting Information—Sect. S6), the zone of inhibition was found to be decreasing with an increase in the treatment time, with no inhibition zones being observed after 195 min, and this is in accordance with the degradation observed (Fig. 2). The decrease in the zone of inhibition suggests the loss of antibiotic activity in the degraded sample.

*LC-MS analysis.* Figure 12a illustrates the HPLC peaks of the initial (pink line) and final (blue line—after 180 min, brown line—after 240 min) CIP samples. The inset graph depicts the MS spectrum of the degraded products. The obtained (experimental)  $m/z$  values were compared with  $m/z$  values in the literature, and the degraded product structures were elucidated (Table 6, Supporting Information Sect. S7).

The possible pathways of CIP degradation using  $B_{0.8}Ce_{0.2}TiO_2/EPS$  film under sunlight are given below in Fig. 12b. The degradation has occurred mainly through the transformation of the piperazine ring, defluorination, decarboxylation, formation of keto derivatives, and finally, less harmful & low molecular weight products were formed. In pathway I, the degradation has occurred via the transformation of the piperazine ring with the formation of  $m/z$ : 263 (degradation of piperazine moiety through the loss of  $CO_2$  from the carboxylate group)  $\rightarrow$  251 (piperazine ring cleavage through loss of  $-C_2H_2$ )  $\rightarrow$  229 (elimination of piperazine moiety). In pathway II, there is formation of the product with  $m/z$ : 315  $\rightarrow$  283, through the loss of F atom (defluorination). In pathway III, the  $m/z$ : 283 was formed by the removal of carboxyl group (decarboxylation). In pathway IV, the formation of keto derivatives has occurred corresponding to the  $m/z$ : 334  $\rightarrow$  291. Finally, the product with  $m/z$ : 200 was formed. Finally, low molecular weight ( $m/z$ : 59) compounds and less harmful products were formed.

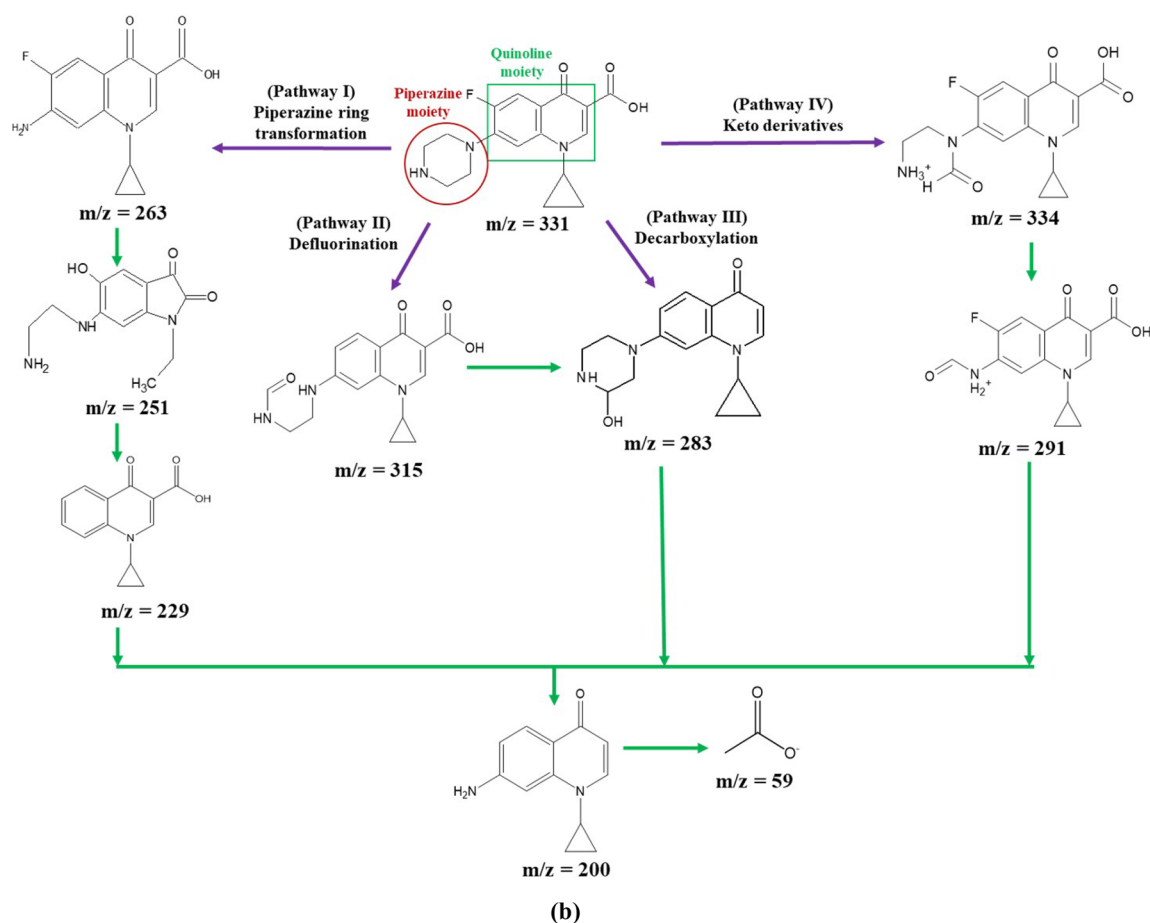
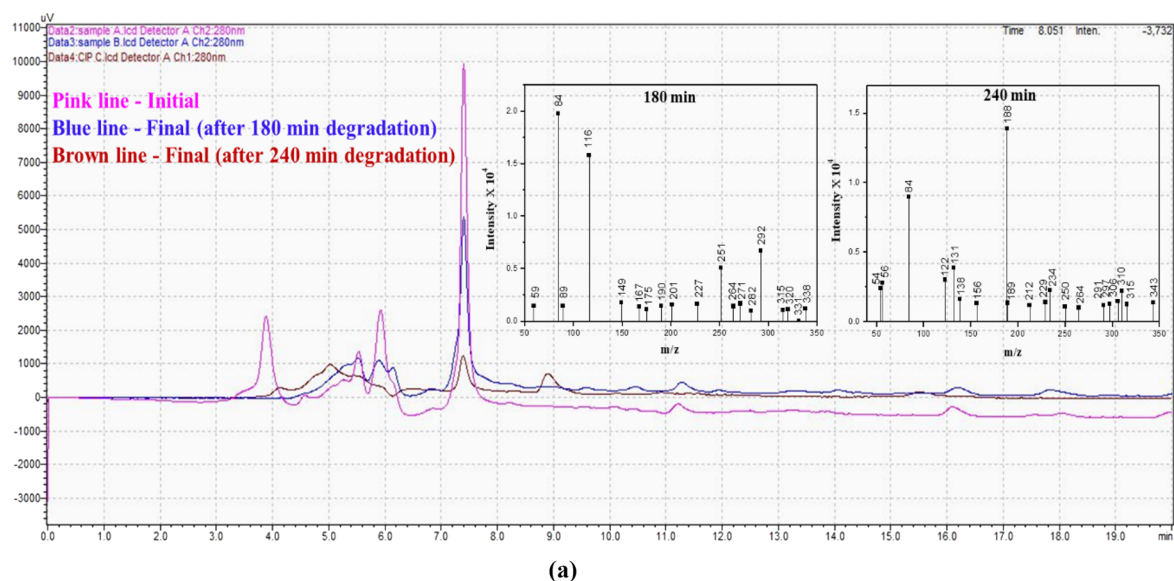


**Figure 12.** (a) HPLC and MS spectrum of CIP degraded products using  $B_{0.8}Ce_{0.2}TiO_2/EPs$  film. (b) Possible degradation pathways of CIP from LC–MS analysis.

**Disinfection studies of the  $B_{0.8}Ce_{0.2}TiO_2/EPs$  film and application in real water matrices.** Figure 13a shows the disinfection of *E. coli* using the /EPs film under sunlight both in the absence and presence of CIP. In the absence of CIP, 6.357 log reduction (99.9999%), and in the presence of CIP, 7.302 log reduction (99.99999%) was observed at the end of 180 min. These results indicate that the immobilized photocatalytic film is quite effective in disinfecting the target micro-organism as these results are in close proximity to the results obtained in the slurry form (7.046 log reduction). The kinetics were studied using the following equation (Eq. 3)<sup>85</sup> using GlnaFit tool. From the kinetics plot of  $\{\log_{10}(N)\}$  (CFU/mL) vs. time (Fig. 13b,c for disinfection

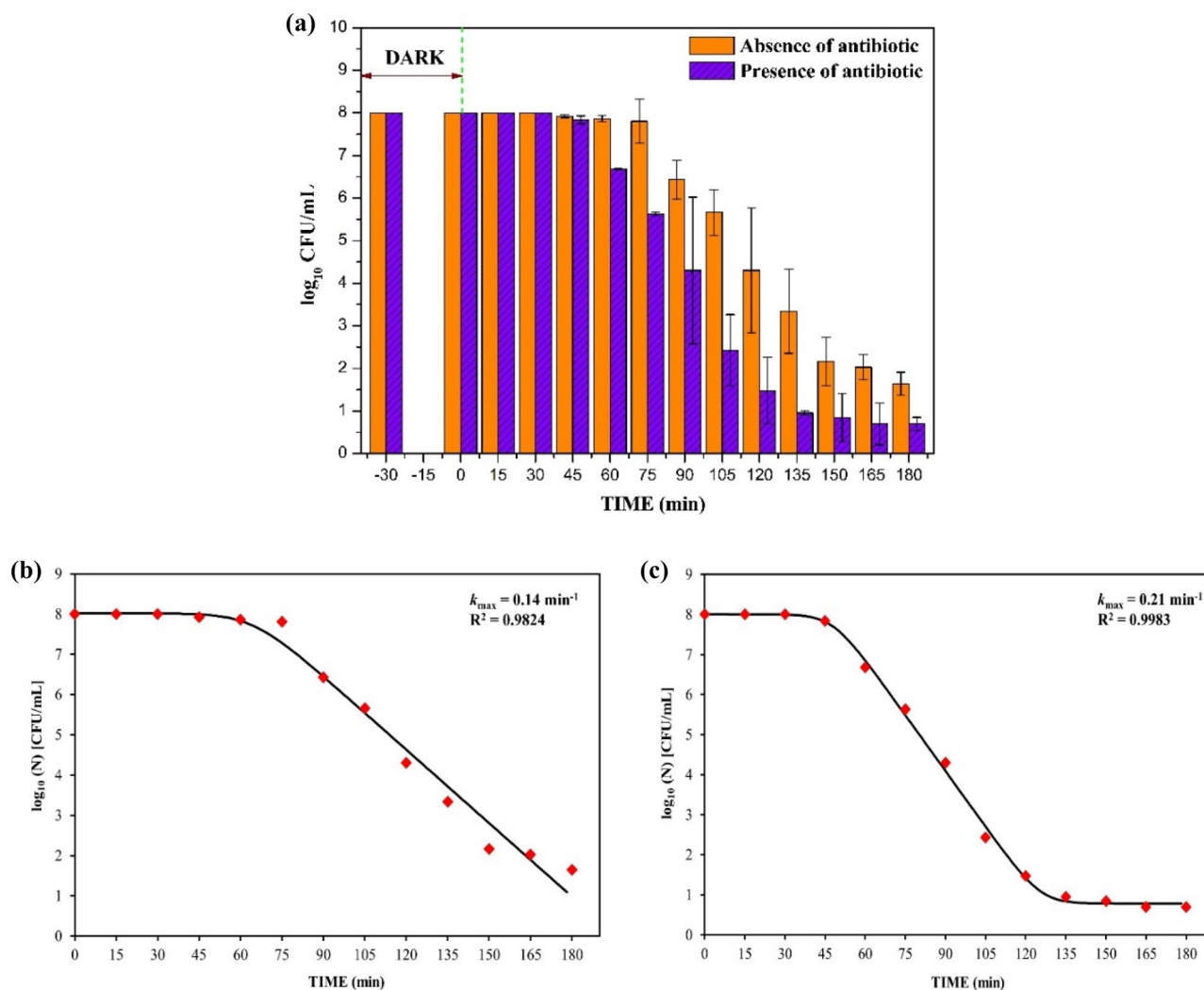


**Figure 13.** (a) Disinfection studies of the immobilized photocatalyst film both in the absence and presence of antibiotic (Initial concentration of *E. coli* =  $10^8$  CFU/mL, 1 ppm CIP, under sunlight). (b) Kinetics plot of disinfection in the absence of antibiotic and (c) Kinetics plot of disinfection in the presence of antibiotic.

in the absence and presence of CIP respectively),  $k_{max}$  and  $R^2$  values are determined (see Table 7, Supporting Information—Sect. S8) which has a shoulder (initial flat portion), linear (center portion), and tail (final flat portion).

$$N(t) = \left( \frac{(N(0) - N_{res}) \times \exp(-k_{max}t) \times (\exp(k_{max} \times Sl))}{(1 + (\exp(k_{max} \times Sl) - 1) \times \exp(-k_{max}t))} \right) + N_{res}, \quad (3)$$

where  $N(t)$  = cell concentration at time  $t$  (CFU/mL),  $N(0)$  = initial cell concentration (CFU/mL),  $t$  = reaction time (min),  $k_{max}$  = rate constant ( $\text{min}^{-1}$ ),  $Sl$  = Shoulder length (as calculated by the tool),  $N_{res}$  = more resistant subpopulation (tail portion, as calculated by the tool).

The  $k_{max}$  values are higher for disinfection in the presence of CIP (antibiotic) when compared to disinfection in the absence of CIP. These results suggest that the disinfection ability of the immobilized film is better even in the presence of antibiotic (CIP), which is essential in the real-water matrix application as it contains both antibiotic residues and superbugs.

The real water samples were spiked with the CIP antibiotic and *E. coli* to determine the performance of the  $\text{B}_{0.8}\text{Ce}_{0.2}\text{TiO}_2/\text{EPS}$  film in the real water matrices. The river water was collected from the Kumaradhara River (Subramanya, Karnataka, India).

The degradation and disinfection (both in the absence and presence of CIP) performance slightly decreased in the real water samples (Fig. 14a,b) when compared to the deionized water. The presence of anions and humic acid (natural organic matter) might hinder the degradation efficiency in the real water samples. As mentioned in the literature<sup>86</sup>, the anions and natural organic matter might react with the generated reactive species and result in a weaker oxidizing agent. Also, the anions could act as scavengers for  $\cdot\text{OH}$  and  $\text{h}^+$  species<sup>87,88</sup>.

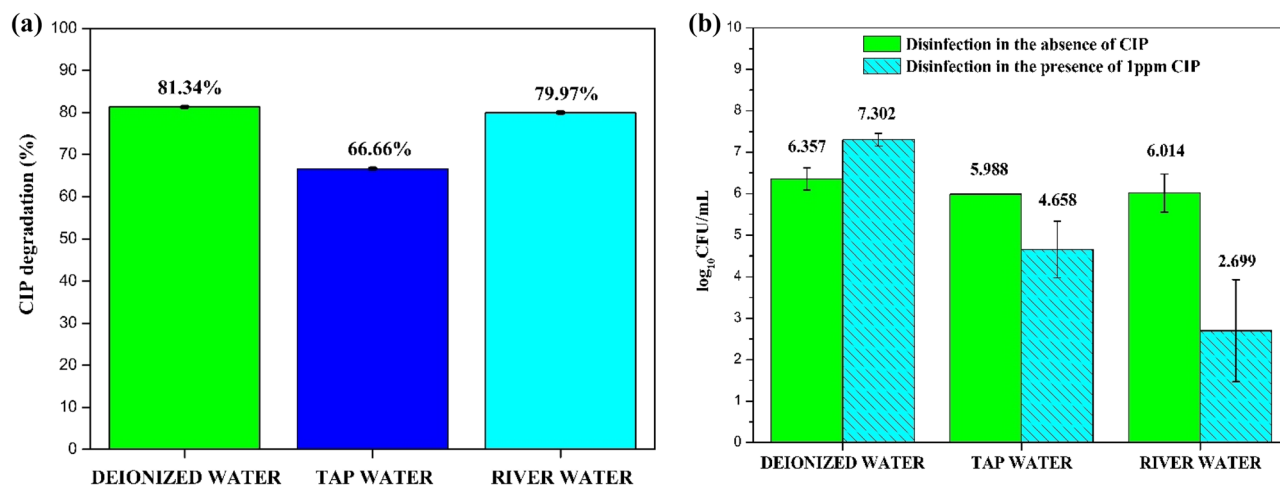


**Figure 14.** (a) CIP degradation using real water samples (10 ppm CIP, 180 min, under sunlight). (b) Disinfection in the absence and presence of 1 ppm CIP using real water samples (180 min, under sunlight).

**Performance of the photocatalyst in suspended and immobilized forms under sunlight and UV-A irradiation.** It is well-known that the suspended form has better photocatalytic performance than the immobilized form due to the available larger surface area in the suspended form. The degradation efficiency obtained in the immobilized form (89.17%, 240 min) is slightly lesser than that of the suspended form (97.43%, 180 min) (Fig. 15a). An increase in the treatment time/longer timeframe can be considered in order to achieve higher efficiency. Moreover, in large-scale application, the immobilized form helps in the reuse of catalysts, thus reducing operating costs.

From Fig. 15b for immobilized form, the degradation efficiency of CIP under sunlight is found to be slightly higher than that under UV-A irradiation. Similar results are reported in the literature<sup>89</sup>.

**Batch scale-up study, effect of H<sub>2</sub>O<sub>2</sub> and degradation of other antibiotics.** A batch scale-up study was performed 550 mL of the CIP solution to determine the effectiveness of the B<sub>0.8</sub>Ce<sub>0.2</sub>TiO<sub>2</sub> immobilized film for treating a larger volume of pollutant solution. The scale-up criteria employed is the ratio of the surface area of the polymer film to reactor volume, and the optimized conditions of the 200 mL were used for the 550 mL reactor. The results are shown in Fig. 16a. The degradation efficiency in both reactor volumes is fairly close to each other, thus confirming the scale-up criteria employed here. However, a slightly higher degradation for the larger reactor volume (~86% degradation at 180 min compared to 225 min for the smaller reactor volume) was observed.

To enhance the degradation activity hydrogen peroxide (H<sub>2</sub>O<sub>2</sub>, an oxidizing agent) was used, and its effect on CIP degradation (at the optimum condition of 20 wt% of catalyst dosage with 200 mL of 10 ppm CIP, and 180 min under sunlight) was examined by varying the concentrations of H<sub>2</sub>O<sub>2</sub> as 0.25, 0.5, 1, 2, and 4 mL per 200 mL CIP solution. In the photocatalytic degradation process, H<sub>2</sub>O<sub>2</sub> has a dual role. It can act as an e<sup>-</sup> scavenger

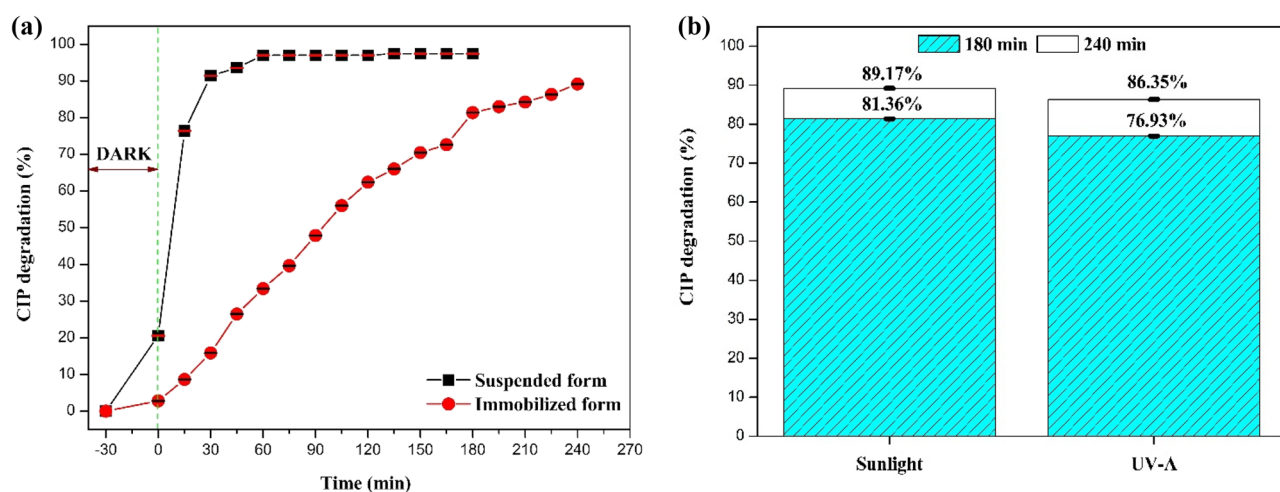


**Figure 15.** (a) Comparison of CIP degradation efficiency in suspended and immobilized forms, (b) Comparison of CIP degradation efficiency under sunlight and UV-A irradiation (immobilized form).

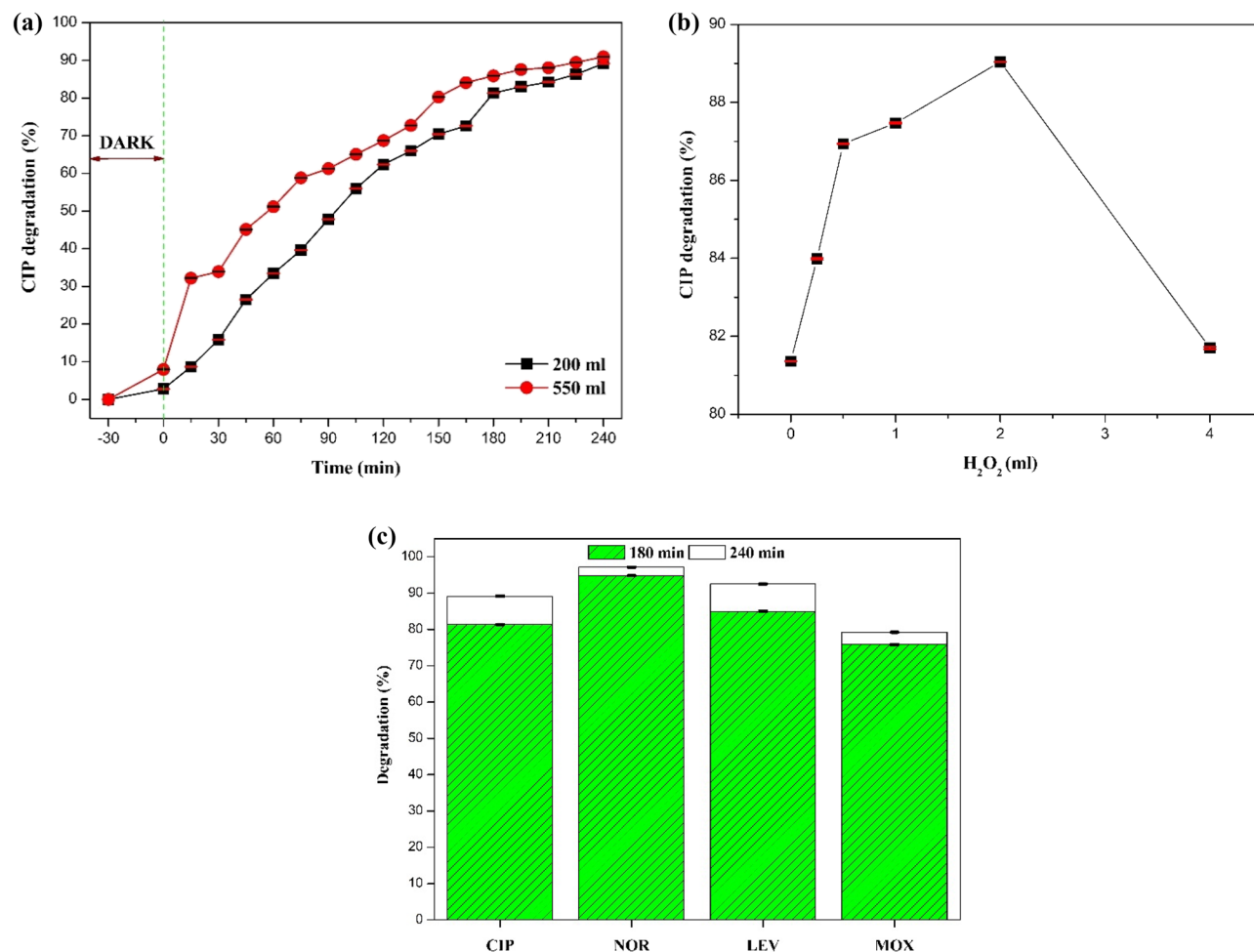


**Figure 16.** (a) Batch reactor scale-up studies using 550 mL of CIP solution under sunlight, (b) effect of H<sub>2</sub>O<sub>2</sub> as an oxidizing agent for 200 ml reactor, and (c) degradation of other antibiotics using the B<sub>0.8</sub>Ce<sub>0.2</sub>TiO<sub>2</sub> immobilized film.

(accepts e<sup>-</sup> from the conduction band), and it also forms ·OH<sup>90,91</sup>. As seen from Fig. 16b, with an increase in the H<sub>2</sub>O<sub>2</sub> concentrations up to 2 mL, the CIP degradation efficiency increased from 81.36 to 89.04% due to the increase in the production of ·OH by H<sub>2</sub>O<sub>2</sub>. However, with an increase in the H<sub>2</sub>O<sub>2</sub> concentration (4 mL), CIP degradation efficiency decreased to 81.07% as scavenging of ·OH occurs due to the reaction between the excess amount of H<sub>2</sub>O<sub>2</sub> and ·OH, according to the following equations (Eqs. 4, 5)<sup>86,92</sup>.



Figure 16c shows the degradation of other antibiotics, such as norfloxacin (NOR), levofloxacin (LEV), and moxifloxacin (MOX), performed using the B<sub>0.8</sub>Ce<sub>0.2</sub>TiO<sub>2</sub> immobilized film under sunlight. The degradation efficiency at the end of 240 min is of the following increasing order: NOR (97.13%) > LEV (92.53%) > CIP (89.17%) > MOX (79.26%). These significant degradation results suggest the effectiveness of the B<sub>0.8</sub>Ce<sub>0.2</sub>TiO<sub>2</sub> immobilized film for the degradation of a broad range of fluoroquinolone antibiotics.

## Conclusions

In this study, a copolymer solar-light active photocatalyst (B<sub>0.8</sub>Ce<sub>0.2</sub>TiO<sub>2</sub>) was immobilized using waste EPS beads. This inert support being buoyant allows for effective utilization of sunlight, and upcycling of the waste EPS reduces the risk of white pollution. The B<sub>0.8</sub>Ce<sub>0.2</sub>TiO<sub>2</sub>/EPS film was employed for the degradation of ciprofloxacin (antibiotic) and disinfection of *E. coli*. From contact angle measurements, after loading of B<sub>0.8</sub>Ce<sub>0.2</sub>TiO<sub>2</sub> photocatalyst, the EPS film behaved as hydrophilic in nature. From XPS analysis, the actual amount of the immobilized photocatalyst was in accordance with the intended/calculated amount during the preparation of the film. The effect of the mixture of solvents in film preparation, the effect of catalyst dosage, and the effect of CIP concentrations on the degradation was studied. The degradation was confirmed through spectrophotometer analysis, TOC reduction, and microbiologically by the residual antimicrobial activity of the degraded ciprofloxacin sample

(well diffusion method). A maximum degradation of 89.17% was observed 240 min respectively at an optimum catalyst dosage of 20 wt% of  $B_{0.8}Ce_{0.2}TiO_2$ . A significant TOC reduction of 84.41% was observed at the end of 240 min. The loss of antimicrobial activity of the degraded CIP sample was confirmed from the decrease of inhibition zones with an increase in the treatment time. From reusability studies, the  $B_{0.8}Ce_{0.2}TiO_2$ /EPS film was found to be stable even after five times of reuse and its application for large-scale purposes. No morphological, structural, and chemical changes in the film were observed (after five times of reuse) as confirmed from FESEM, XRD, and FTIR analysis, respectively. Minute traces of doped elements (B and Ce) were observed from ICP-OES analysis (leaching study). Effective and promising results were observed for the degradation and disinfection studies carried out using real water samples. A slightly higher degradation (90.96% at the end of 240 min) was observed for the larger reactor volume (550 mL). These immobilized films were effective against a broad range of fluoroquinolone antibiotics. These results suggest the efficacy of the EPS film in terms of both degradation and disinfection under sunlight which can serve as a sustainable tool for the emerging global antimicrobial resistance. Effectiveness of  $B_{0.8}Ce_{0.2}TiO_2$ /EPS film using real water samples, and broad range of antibiotics clearly indicates its suitability for real-world applications with mixture of antibiotics in waterbodies. In comparison with similar works involving polystyrene or other supports for immobilization (Tables 1, 2, Supporting Information, S1), it is evident that the  $B_{0.8}Ce_{0.2}TiO_2$ /EPS film is as efficient or perhaps better than some of the latest generation photocatalysts. Moreover, the upcycled EPS beads contributes to minimizing the ‘white pollution’ as mentioned earlier. Further, these immobilized films can be employed for simultaneous degradation and disinfection studies which are essential to solve the problem of antimicrobial resistance. Also, reactor studies can be carried out using the EPS film for large-scale applications.

### Data availability

All data generated or analysed during this study are included in this published article (and its Supplementary Information files).

Received: 31 May 2023; Accepted: 30 August 2023

Published online: 05 September 2023

### References

- [https://www.usgs.gov/special-topic/water-science-school/science/how-much-water-there-earth?qt-science\\_center\\_objects=0#qt-science\\_center\\_objects](https://www.usgs.gov/special-topic/water-science-school/science/how-much-water-there-earth?qt-science_center_objects=0#qt-science_center_objects) (Accessed 07 May 2021).
- Herman, R. *Emerging Contaminants Taint Drinking Water Supply*. <https://blogs.scientificamerican.com/guest-blog/emerging-contaminants-taint-drinking-water-supply/> (2022).
- Deegan, A. M. *et al.* Treatment options for wastewater effluents from pharmaceutical companies. *Int. J. Environ. Sci. Technol.* **8**(3), 649–666. <https://doi.org/10.1007/BF03326250> (2011).
- Fujishima, A. & Zhang, X. Titanium dioxide photocatalysis: Present situation and future approaches. *C. R. Chim.* **9**, 750–760. <https://doi.org/10.1016/j.crci.2005.02.055> (2006).
- Munter, R. Advanced oxidation processes—Current status and prospects. *Proc. Est. Acad. Sci. Chem.* **50**(2), 59–80. <https://doi.org/10.1002/CHIN.200141291> (2001).
- Huang, F., Yan, A. & Zhao, H. Influences of doping on photocatalytic properties of  $TiO_2$  photocatalyst. In *Semiconductor Photocatalysis Materials, Mechanisms and Applications* (ed. Cao, W.) 31–80 (InTech, 2016).
- Wang, Y. *et al.* Recent advances in visible-light driven photocatalysis. In *Advanced Catalytic Materials Photocatalysis and Other Current Trends* (eds Norena, L. E. & Wang, J.-A.) 337–357 (InTech, 2016).
- Jaiswal, R. *et al.* Efficient Co-B-codoped  $TiO_2$  photocatalyst for degradation of organic water pollutant under visible light. *Appl. Catal. B Environ.* **183**, 242–253. <https://doi.org/10.1016/j.apcatb.2015.10.041> (2016).
- Marschall, R. & Wang, L. Non-metal doping of transition metal oxides for visible-light photocatalysis. *Catal. Today* **225**, 111–135. <https://doi.org/10.1016/j.cattod.2013.10.088> (2014).
- Wang, Y., Wu, Y., Yang, H., Xue, X. & Liu, Z. Doping  $TiO_2$  with boron or/and cerium elements: Effects on photocatalytic antimicrobial activity. *Vacuum* **131**, 58–64. <https://doi.org/10.1016/j.vacuum.2016.06.003> (2016).
- Wang, Y. Z. *et al.* Effect of calcination temperature on the microstructure and antimicrobial activity of boron and cerium codoped titania nanomaterials. *Mater. Technol.* **33**(1), 48–56. <https://doi.org/10.1080/10667857.2017.1389051> (2018).
- Srikanth, B. *et al.* Recent advancements in supporting materials for immobilised photocatalytic applications in waste water treatment. *J. Environ. Manag.* **200**, 60–78. <https://doi.org/10.1016/j.jenvman.2017.05.063> (2017).
- Xing, Z. *et al.* Recent advances in floating  $TiO_2$ -based photocatalysts for environmental application. *Appl. Catal. B Environ.* **225**, 452–467. <https://doi.org/10.1016/j.apcatb.2017.12.005> (2018).
- Shan, A. Y., Ghazi, T. I. M. & Rashid, S. A. Immobilisation of titanium dioxide onto supporting materials in heterogeneous photocatalysis: A review. *Appl. Catal. A Gen.* **389**(1–2), 1–8. <https://doi.org/10.1016/j.apcata.2010.08.053> (2010).
- Sboui, M., Nsib, M. F., Rayes, A., Swaminathan, M. & Houas, A.  $TiO_2$ -PANI/Cork composite: A new floating photocatalyst for the treatment of organic pollutants under sunlight irradiation. *J. Environ. Sci.* **60**, 3–13. <https://doi.org/10.1016/j.jes.2016.11.024> (2017).
- Długosz, M. *et al.* Photocatalytic degradation of sulfamethoxazole in aqueous solution using a floating  $TiO_2$ -expanded perlite photocatalyst. *J. Hazard. Mater.* **298**, 146–153. <https://doi.org/10.1016/j.jhazmat.2015.05.016> (2015).
- Hosseini, S. N., Borghei, S. M., Vossoughi, M. & Taghavinia, N. Immobilization of  $TiO_2$  on perlite granules for photocatalytic degradation of phenol. *Appl. Catal. B Environ.* **74**(1–2), 53–62. <https://doi.org/10.1016/j.apcatb.2006.12.015> (2007).
- Ata, R. *et al.* Visible light active N-doped  $TiO_2$  immobilized on polystyrene as efficient system for wastewater treatment. *J. Photochem. Photobiol. A Chem.* **348**, 255–262. <https://doi.org/10.1016/j.jphotochem.2017.08.054> (2017).
- Duca, C., Imoberdorf, G. E. & Mohseni, M. Synthesis, characterization, and comparison of solgel  $TiO_2$  immobilized photocatalysts. *Int. J. Chem. React. Eng.* **11**(2), 633–639. <https://doi.org/10.1515/ijcre-2012-0054> (2013).
- Zhang, J. *et al.*  $TiO_2$ /T-PVA composites immobilized on cordierite: Structure and photocatalytic activity for degrading RhB under visible light. *Water. Air. Soil Pollut.* **224**(7), 8. <https://doi.org/10.1007/s11270-013-1555-8> (2013).
- Sökmen, M. *et al.* A new nano- $TiO_2$  immobilized biodegradable polymer with self-cleaning properties. *J. Hazard. Mater.* **187**(1–3), 199–205. <https://doi.org/10.1016/j.jhazmat.2011.01.020> (2011).
- Nawawi, W., Zaharudin, R., Ishak, M., Ismail, K. & Zuliahani, A. The preparation and characterization of immobilized  $TiO_2$ /PEG by using DSAT as a support binder. *Appl. Sci.* **7**(1), 24. <https://doi.org/10.3390/app7010024> (2016).

23. Koysuren, O. & Koysuren, H. N. Photocatalytic activities of poly(methyl methacrylate)/titanium dioxide nanofiber. *Mater. J. Macromol. Sci. A* **54**(2), 80–84. <https://doi.org/10.1080/10601325.2017.1261619> (2017).
24. Colmenares, J. C. & Kuna, E. Photoactive hybrid catalysts based on natural and synthetic polymers: A comparative overview. *Molecules* **22**(5), 790 (2017).
25. Rtimi, S. *et al.* Innovative transparent non-scattering TiO<sub>2</sub> bactericide thin films inducing increased *E. coli* cell wall fluidity. *Surf. Coat. Technol.* **254**, 333–343. <https://doi.org/10.1016/j.surfcoat.2014.06.035> (2014).
26. Rtimi, S. & Kiwi, J. Bactericide effects of transparent polyethylene photocatalytic films coated by oxides under visible light. *Appl. Catal. B Environ.* **213**, 62–73. <https://doi.org/10.1016/j.apcatb.2017.05.004> (2017).
27. Singh, S., Mahalingam, H. & Singh, P. K. Polymer-supported titanium dioxide photocatalysts for environmental remediation: A review. *Appl. Catal. A* **462–463**, 178–195. <https://doi.org/10.1016/j.apcata.2013.04.039> (2013).
28. Daneshvar, N., Salari, D., Niaei, A. & Rasoulifard, M. H. Immobilization of TiO<sub>2</sub> nanopowder on glass beads for the photocatalytic decolorization of an azo dye C.I direct red 23. *J. Environ. Sci. Health A* **40**(8), 1605–1617. <https://doi.org/10.1081/ESE-200060664> (2005).
29. Xing, X., Du, Z., Zhuang, J. & Wang, D. Removal of ciprofloxacin from water by nitrogen doped TiO<sub>2</sub> immobilized on glass spheres: Rapid screening of degradation products. *J. Photochem. Photobiol. A Chem.* **359**, 23–32. <https://doi.org/10.1016/j.jphotochem.2018.03.026> (2018).
30. Cunha, D. L., Kuznetsov, A., Achete, C. A., da Machado, A. E. H. & Marques, M. Immobilized TiO<sub>2</sub> on glass spheres applied to heterogeneous photocatalysis: Photoactivity, leaching and regeneration process. *PeerJ* **6**, e4464. <https://doi.org/10.7717/peerj.4464> (2018).
31. Shen, C., Pang, K., Du, L. & Luo, G. Green synthesis and enhanced photocatalytic activity of Ce-doped TiO<sub>2</sub> nanoparticles supported on porous glass. *Particology* **34**, 103–109. <https://doi.org/10.1016/j.partic.2017.01.007> (2017).
32. Gou, J. *et al.* Fabrication of Ag<sub>2</sub>O/TiO<sub>2</sub>-zeolite composite and its enhanced solar light photocatalytic performance and mechanism for degradation of norfloxacin. *Chem. Eng. J.* **308**, 818–826. <https://doi.org/10.1016/j.cej.2016.09.089> (2017).
33. Li, H., Zhang, W. & Liu, Y. HZSM-5 zeolite supported boron-doped TiO<sub>2</sub> for photocatalytic degradation of ofloxacin. *J. Mater. Res. Technol.* **9**(2), 2557–2567. <https://doi.org/10.1016/j.jmrt.2019.12.086> (2020).
34. Paul, B., Martens, W. N. & Frost, R. L. Immobilised anatase on clay mineral particles as a photocatalyst for herbicides degradation. *Appl. Clay Sci.* **57**, 49–54. <https://doi.org/10.1016/j.clay.2011.12.009> (2012).
35. De Oliveira, W. V. *et al.* TiO<sub>2</sub> immobilized on fibrous clay as strategies to photocatalytic activity. *Mater. Res.* **23**(1), 1–10. <https://doi.org/10.1590/1980-5373-MR-2019-0463> (2020).
36. Zhao, Y., Tao, C., Xiao, G. & Su, H. Controlled synthesis and wastewater treatment of Ag<sub>2</sub>O/TiO<sub>2</sub> modified chitosan-based photocatalytic film. *RSC Adv.* **7**(18), 11211–11221. <https://doi.org/10.1039/C6RA27295A> (2017).
37. Sarkar, S., Chakraborty, S. & Bhattacharjee, C. Photocatalytic degradation of pharmaceutical wastes by alginate supported TiO<sub>2</sub> nanoparticles in packed bed photo reactor (PBPR). *Ecotoxicol. Environ. Saf.* **121**, 263–270. <https://doi.org/10.1016/j.ecoenv.2015.02.035> (2015).
38. Dalponte, I., de Sousa, B. C., Mathias, A. L. & Matos Jorge, R. M. Formulation and optimization of a novel TiO<sub>2</sub>/calcium alginate floating photocatalyst. *Int. J. Biol. Macromol.* **137**, 992–1001. <https://doi.org/10.1016/j.ijbiomac.2019.07.020> (2019).
39. Cámara, R. M., Portela, R., Gutiérrez-Martín, F. & Sánchez, B. Evaluation of several commercial polymers as support for TiO<sub>2</sub> in photocatalytic applications. *Glob. NEST J.* **16**(3), 525–535 (2014).
40. Mangalara, S. C. H. & Varughese, S. Green recycling approach to obtain nano- and microparticles from expanded polystyrene waste. *ACS Sustain. Chem. Eng.* **4**(11), 6095–6100. <https://doi.org/10.1021/acssuschemeng.6b01493> (2016).
41. Wang, X. *et al.* An Alternative to in situ photocatalytic degradation of microcystin-LR by worm-like N, P codoped TiO<sub>2</sub>/expanded graphite by carbon layer (NPT-EGC) floating composites. *Appl. Catal. B Environ.* **206**, 479–489. <https://doi.org/10.1016/j.apcatb.2017.01.046> (2017).
42. Singh, S., Chaki, A., Chand, D. P., Raghuvanshi, A. & Singh, P. K. A novel polystyrene-supported titanium dioxide photocatalyst for degradation of methyl orange and methylene blue dyes under UV irradiation. *J. Chem. Eng.* **28**(1), 9–13. <https://doi.org/10.3329/jce.v28i1.18103> (2014).
43. Das, S. & Mahalingam, H. Reusable floating polymer nanocomposite photocatalyst for the efficient treatment of dye wastewaters under scaled-up conditions in batch and recirculation modes. *J. Chem. Technol. Biotechnol.* **94**(8), 2597–2608. <https://doi.org/10.1002/jctb.6069> (2019).
44. Padervand, M., Lichtfouse, E., Robert, D. & Wang, C. Removal of microplastics from the environment. A review. *Environ. Chem. Lett.* **18**, 807–828. <https://doi.org/10.1007/s10311-020-00983-1> (2020).
45. Mohsen Padervand, M. *United States Patent Padervand: US11014082 B2: May 25, 2021.* <https://patents.google.com/patent/US11014082B2/en>. (Accessed 25 May 2021).
46. Singh, S., Singh, P. K. & Mahalingam, H. An effective and low-cost TiO<sub>2</sub>/polystyrene floating photocatalyst for environmental remediation. *Int. J. Environ. Res.* **9**(2), 535–544 (2015).
47. Singh, G. D. & Gupta, K. C. Photo and UV degradation of ciprofloxacin antibiotic. *Int. J. Curr. Microbiol. Appl. Sci.* **3**(6), 641–648 (2014).
48. Magalhães, F. & Lago, R. M. Floating photocatalysts based on TiO<sub>2</sub> grafted on expanded polystyrene beads for the solar degradation of dyes. *Sol. Energy* **83**(9), 1521–1526. <https://doi.org/10.1016/j.solener.2009.04.005> (2009).
49. Vaiano, V., Matarangolo, M. & Sacco, O. UV-LEDs floating-bed photoreactor for the removal of caffeine and paracetamol using ZnO supported on polystyrene pellets. *Chem. Eng. J.* **350**, 703–713. <https://doi.org/10.1016/j.cej.2018.06.011> (2018).
50. Lee, Y. J., Lee, C. G., Kang, J. K., Park, S. J. & Alvarez, P. J. J. Simple preparation method for styrofoam-TiO<sub>2</sub> composites and their photocatalytic application for dye oxidation and Cr (VI) reduction in industrial wastewater. *Environ. Sci. Water Res. Technol.* **7**(1), 222–230. <https://doi.org/10.1039/d0ew00787k> (2021).
51. Fabyi, M. E. & Skelton, R. L. Photocatalytic mineralisation of methylene blue using buoyant TiO<sub>2</sub>-coated polystyrene beads. *J. Photochem. Photobiol. A Chem.* **132**, 121–128. [https://doi.org/10.1016/S1010-6030\(99\)00250-6](https://doi.org/10.1016/S1010-6030(99)00250-6) (2000).
52. Varnagir, S. *et al.* Floating TiO<sub>2</sub> photocatalyst for efficient inactivation of *E. coli* and decomposition of methylene blue solution. *Sci. Total Environ.* **720**, 137600. <https://doi.org/10.1016/j.scitotenv.2020.137600> (2020).
53. Das, S. & Mahalingam, H. Dye degradation studies using immobilized pristine and waste polystyrene-TiO<sub>2</sub>/rGO/g-C<sub>3</sub>N<sub>4</sub> nanocomposite photocatalytic film in a novel airlift reactor under solar light. *J. Environ. Chem. Eng.* **7**(5), 103289. <https://doi.org/10.1016/j.jece.2019.103289> (2019).
54. Liu, S. H., Lu, C. C., Lin, C. W. & Chang, S. H. Rapid modification of waste expanded polystyrene with H<sub>2</sub>SO<sub>4</sub>/trace persulfate in one pot for effective adsorption of fluoroquinolone antibiotic and its regeneration. *Chemosphere* **271**, 129529. <https://doi.org/10.1016/j.chemosphere.2020.129529> (2021).
55. Manjunatha, M., Chandewar, P. R. & Mahalingam, H. Exploring the synergy of B, Ce dopants in codoped titanium dioxide multifunctional photocatalysts for antibiotic degradation and microbial disinfection under solar light. *Phys. Status Solidi Appl. Mater. Sci.* **219**, 2100581. <https://doi.org/10.1002/pssa.202100581> (2022).
56. Abass, A. K. Effect type of solvent, type of catalyst and power of lamp on photo oxidation of benzene. *J. Univ. Babylon Eng. Sci.* **26**(10), 197–207 (2018).
57. Johanson, G. Acetone. *Patty Toxicol.* **3**, 735–752. <https://doi.org/10.1002/0471435139.tox074.pub2> (2012).

58. Wankasi, D. & Dikio, E. D. Comparative study of polystyrene and polymethylmethacrylate wastes as adsorbents for sorption of Pb<sup>2+</sup> from aqueous solution. *Asian J. Chem.* **26**(24), 8295–8302 (2014).
59. Vieira, G. B. *et al.* CeO<sub>2</sub>/TiO<sub>2</sub> nanostructures enhance adsorption and photocatalytic degradation of organic compounds in aqueous suspension. *J. Photochem. Photobiol. A Chem.* **353**, 325–336. <https://doi.org/10.1016/j.jphotochem.2017.11.045> (2018).
60. Zhao, S. *et al.* The performance and mechanism of Ag-doped CeO<sub>2</sub>/TiO<sub>2</sub> catalysts in the catalytic oxidation of gaseous elemental mercury. *Catal. Sci. Technol.* **5**(5), 2985–2993. <https://doi.org/10.1039/c4cy01745e> (2015).
61. Allah, M. A. H. D., Taqui, S. N., Syed, U. T. & Syed, A. A. Development of sustainable acid blue 113 dye adsorption system using nutraceutical industrial *Tribulus terrestris* spent. *SN Appl. Sci.* **1**, 5. <https://doi.org/10.1007/s42452-018-0125-5> (2019).
62. Zakharova, G. S. *et al.* TiO<sub>2</sub>/C nanocomposites prepared by thermal annealing of titanium glycerolate as anode materials for lithium-ion batteries. *J. Mater. Sci.* **53**(17), 12244–12253. <https://doi.org/10.1007/s10853-018-2488-9> (2018).
63. Li, W., Liang, R., Hu, A., Huang, Z. & Zhou, Y. N. Generation of oxygen vacancies in visible light activated one-dimensional iodine TiO<sub>2</sub> photocatalysts. *RSC Adv.* **4**(70), 36959–36966. <https://doi.org/10.1039/c4ra04768k> (2014).
64. Wen, X. J. *et al.* Study of the photocatalytic degradation pathway of norfloxacin and mineralization activity using a novel ternary Ag/AgCl–CeO<sub>2</sub> photocatalyst. *J. Catal.* **355**, 73–86. <https://doi.org/10.1016/j.jcat.2017.08.028> (2017).
65. Wen, X. J. *et al.* Photocatalytic degradation of ciprofloxacin by a novel Z-scheme CeO<sub>2</sub>–Ag/AgBr photocatalyst: Influencing factors, possible degradation pathways, and mechanism insight. *J. Catal.* **358**, 141–154. <https://doi.org/10.1016/j.jcat.2017.11.029> (2018).
66. Aponte, Á. G., Ramírez, M. A. L., Mora, Y. C., Marín, J. F. S. & Sierra, R. B. Cerium oxide nanoparticles for color removal of indigo carmine and methylene blue solutions. *AIMS Mater. Sci.* **7**(4), 468–485. <https://doi.org/10.3934/mat.2020.4.468> (2020).
67. Maarisetty, D. & Baral, S. S. Defect-induced enhanced dissociative adsorption, optoelectronic properties and interfacial contact in Ce doped TiO<sub>2</sub>: Solar photocatalytic degradation of rhodamine B. *Ceram. Int.* **45**(17), 22253–22263. <https://doi.org/10.1016/j.ceramint.2019.07.251> (2019).
68. Feng, N. *et al.* Boron environments in B-doped and (B, N) -codoped TiO<sub>2</sub> photocatalysts: A combined solid-state NMR and theoretical calculation study. *J. Phys. Chem. C* **115**, 2709–2719. <https://doi.org/10.1021/jp108008a> (2011).
69. Patel, N. *et al.* Experimental and theoretical investigations on the activity and stability of substitutional and interstitial boron in TiO<sub>2</sub> photocatalyst. *J. Phys. Chem. C* **119**(32), 18581–18590. <https://doi.org/10.1021/acs.jpcc.5b05290> (2015).
70. Liu, Z., Guo, B., Hong, L. & Jiang, H. Preparation and characterization of cerium oxide doped TiO<sub>2</sub> nanoparticles. *J. Phys. Chem. Solids* **66**(1), 161–167. <https://doi.org/10.1016/j.jpcc.2004.09.002> (2005).
71. World Health Organization. *Guidelines for Drinking-Water Quality* 3rd edn, 306 (WHO Press, 2008).
72. Dong, S. Z., Chen, C. Z., Li, D. M. & Sun, Y. S. A study of hygienic standard for titanium in the source of drinking water. *Chin. J. Prev. Med.* **27**, 26–28 (1993).
73. Das, S. *et al.* Sunlight assisted photocatalytic degradation of ciprofloxacin in water using Fe doped ZnO nanoparticles for potential public health applications. *Int. J. Environ. Res. Public Health* **15**(11), 1–11. <https://doi.org/10.3390/ijerph15112440> (2018).
74. Shetty, R., Chavan, V. B., Kulkarni, P. S., Kulkarni, B. D. & Kamble, S. P. Photocatalytic degradation of pharmaceuticals pollutants using N-doped TiO<sub>2</sub> photocatalyst: Identification of CFX degradation intermediates. *Indian Chem. Eng.* **59**(3), 177–199. <https://doi.org/10.1080/00194506.2016.1150794> (2017).
75. Shah, N. S. *et al.* Solar light driven degradation of norfloxacin using as-synthesized Bi<sup>3+</sup> and Fe<sup>2+</sup> codoped ZnO with the addition of HSO<sub>3</sub><sup>-</sup>: Toxicities and degradation pathways investigation. *Chem. Eng. J.* **351**, 841–855. <https://doi.org/10.1016/j.cej.2018.06.111> (2018).
76. Sayed, M. *et al.* Solar light responsive poly(vinyl alcohol)-assisted hydrothermal synthesis of immobilized TiO<sub>2</sub>/Ti film with the addition of peroxymonosulfate for photocatalytic degradation of ciprofloxacin in aqueous media: A mechanistic approach. *J. Phys. Chem. C* **122**(1), 406–421. <https://doi.org/10.1021/acs.jpcc.7b09169> (2018).
77. Hassani, A., Khataee, A., Karaca, S., Karaca, C. & Gholami, P. Sonocatalytic degradation of ciprofloxacin using synthesized TiO<sub>2</sub> nanoparticles on montmorillonite. *Ultrason. Sonochem.* **35**, 251–262. <https://doi.org/10.1016/j.ultrsonch.2016.09.027> (2017).
78. Geeraerd, A. H., Herremans, C. H. & Van Impe, J. F. Structural model requirements to describe microbial inactivation during a mild heat treatment. *Int. J. Food Microbiol.* **59**(3), 185–209. [https://doi.org/10.1016/S0168-1605\(00\)00362-7](https://doi.org/10.1016/S0168-1605(00)00362-7) (2000).
79. Wang, C., Zhu, L., Wei, M., Chen, P. & Shan, G. Photolytic reaction mechanism and impacts of coexisting substances on photo-degradation of bisphenol A by Bi<sub>2</sub>WO<sub>6</sub> in water. *Water Res.* **46**(3), 845–853. <https://doi.org/10.1016/j.watres.2011.11.057> (2012).
80. Wang, J. *et al.* Atomic scale g-C<sub>3</sub>N<sub>4</sub>/Bi<sub>2</sub>WO<sub>6</sub> 2D/2D heterojunction with enhanced photocatalytic degradation of ibuprofen under visible light irradiation. *Appl. Catal. B Environ.* **209**, 285–294. <https://doi.org/10.1016/j.apcatb.2017.03.019> (2017).
81. Sarafraz, M. *et al.* Enhanced photocatalytic degradation of ciprofloxacin by black Ti<sup>3+</sup>/N-TiO<sub>2</sub> under visible LED light irradiation: Kinetic, energy consumption, degradation pathway, and toxicity assessment. *Process Saf. Environ. Prot.* **137**, 261–272. <https://doi.org/10.1016/j.psep.2020.02.030> (2020).
82. Bosio, M., Satyro, S., Bassin, J. P., Saggiaro, E. & Dezotti, M. Removal of pharmaceutically active compounds from synthetic and real aqueous mixtures and simultaneous disinfection by supported TiO<sub>2</sub>/UV-A, H<sub>2</sub>O<sub>2</sub>/UV-A, and TiO<sub>2</sub>/H<sub>2</sub>O<sub>2</sub>/UV-A processes. *Environ. Sci. Pollut. Res.* **26**, 4288–4299. <https://doi.org/10.1007/s11356-018-2108-x> (2019).
83. Chen, J., Liu, M., Zhang, J., Ying, X. & Jin, L. Photocatalytic degradation of organic wastes by electrochemically assisted TiO<sub>2</sub> photocatalytic system. *J. Environ. Manage.* **70**(1), 43–47. <https://doi.org/10.1016/j.jenvman.2003.09.019> (2004).
84. Bizani, E., Fytianos, K., Poullos, I. & Tsiridis, V. Photocatalytic decolorization and degradation of dye solutions and wastewaters in the presence of titanium dioxide. *J. Hazard. Mater.* **136**(1), 85–94. <https://doi.org/10.1016/j.jhazmat.2005.11.017> (2006).
85. Dönmez, Ö., Dükkancı, M. & Gündüz, G. Effects of catalyst preparation method and reaction parameters on the ultrasound assisted photocatalytic oxidation of reactive yellow 84 dye. *J. Environ. Health Sci. Eng.* **18**(2), 835–851. <https://doi.org/10.1007/s40201-020-00507-7> (2020).
86. Das, S. & Mahalingam, H. Exploring the synergistic interactions of TiO<sub>2</sub>, rGO, and g-C<sub>3</sub>N<sub>4</sub> catalyst admixtures in a polystyrene nanocomposite photocatalytic film for wastewater treatment: Unary, binary and ternary systems. *J. Environ. Chem. Eng.* **7**(4), 103246. <https://doi.org/10.1016/j.jece.2019.103246> (2019).
87. Wang, J. *et al.* Atomic scale g-C<sub>3</sub>N<sub>4</sub>/Bi<sub>2</sub>WO<sub>6</sub> 2D/2D heterojunction with enhanced photocatalytic degradation of ibuprofen under visible light irradiation. *Appl. Catal. B Environ.* **209**, 285–294. <https://doi.org/10.1016/j.apcatb.2017.03.019> (2017).
88. Sarafraz, M. *et al.* Enhanced photocatalytic degradation of ciprofloxacin by black Ti<sub>3</sub><sup>+</sup>/N-TiO<sub>2</sub> under visible LED light irradiation: Kinetic, energy consumption, degradation pathway, and toxicity assessment. *Process Saf. Environ. Prot.* **137**, 261–272. <https://doi.org/10.1016/j.psep.2020.02.030> (2020).
89. Bosio, M., Satyro, S., Bassin, J.P., Saggiaro, E. & Dezotti, M. Removal of pharmaceutically active compounds from synthetic and real aqueous mixtures and simultaneous disinfection by supported TiO<sub>2</sub>/UV-A H<sub>2</sub>O<sub>2</sub>/UV-A and TiO<sub>2</sub>/H<sub>2</sub>O<sub>2</sub>/UV-A processes. *Environ. Sci. Pollut. Res.* **26**(5) 4288–4299. <https://doi.org/10.1007/s11356-018-2108-x> (2019).
90. Chen, J., Liu, M., Zhang, J., Ying, X. & Jin, L. Photocatalytic degradation of organic wastes by electrochemically assisted TiO<sub>2</sub> photocatalytic system. *J. Environ. Manage.* **70**(1), 43–47. <https://doi.org/10.1016/j.jenvman.2003.09.019> (2004).
91. Bizani, E., Fytianos, K., Poullos, I. & Tsiridis, V. Photocatalytic decolorization and degradation of dye solutions and wastewaters in the presence of titanium dioxide. *J. Hazard. Mater.* **136**(1), 85–94. <https://doi.org/10.1016/j.jhazmat.2005.11.017> (2006).
92. Dönmez, Ö., Dükkancı, M. & Gündüz, G. Effects of catalyst preparation method and reaction parameters on the ultrasound assisted Photocatalytic oxidation of reactive yellow 84 dye. *J. Environ. Health Sci. Eng.* **18**, 835–851. <https://doi.org/10.1007/s40201-020-00507-7> (2020).

## Acknowledgements

The author would like to thank the Ministry of Education, Government of India, for scholarship. Also, thanks are due to the following organizations: CRF-NITK for FESEM analysis, Dr. Narayan Prabhu, Department of Metallurgy and Materials engineering, NITK for contact angle analysis and MNIT, Jaipur for XPS analysis.

## Author contributions

M.M. performed the experiments, data analysis and wrote the first draft of the manuscript. H.M. supervised the research work and edited/revised the manuscript. All authors reviewed the manuscript.

## Competing interests

The authors declare no competing interests.

## Additional information

**Supplementary Information** The online version contains supplementary material available at <https://doi.org/10.1038/s41598-023-41705-1>.

**Correspondence** and requests for materials should be addressed to H.M.

**Reprints and permissions information** is available at [www.nature.com/reprints](http://www.nature.com/reprints).

**Publisher's note** Springer Nature remains neutral with regard to jurisdictional claims in published maps and institutional affiliations.



**Open Access** This article is licensed under a Creative Commons Attribution 4.0 International License, which permits use, sharing, adaptation, distribution and reproduction in any medium or format, as long as you give appropriate credit to the original author(s) and the source, provide a link to the Creative Commons licence, and indicate if changes were made. The images or other third party material in this article are included in the article's Creative Commons licence, unless indicated otherwise in a credit line to the material. If material is not included in the article's Creative Commons licence and your intended use is not permitted by statutory regulation or exceeds the permitted use, you will need to obtain permission directly from the copyright holder. To view a copy of this licence, visit <http://creativecommons.org/licenses/by/4.0/>.

© The Author(s) 2023